INTRAMOLECULAR THROUGH-SPACE CHARGE-TRANSFER IN NAPHTHALENE-BASED COMPOUNDS AND DEVELOPMENT OF AN EFFICIENT HETEROGENEOUS CATALYTIC METHOD FOR THE AEROBIC C-H OXIDATION OF ALKYLARENES

A THESIS SUBMITTED TO

THE GRADUATE SCHOOL OF ENGINEERING AND SCIENCE OF

BILKENT UNIVERSITY

IN PARTIAL FULFILLMENT OF THE REQUIREMENTS FOR THE DEGREE

OF

MASTER OF SCIENCE IN

CHEMISTRY

By

Eylül Çalıkyılmaz

September 2023

Advisor: Yunus Emre Türkmen

INTRAMOLECULAR THROUGH-SPACE CHARGE-TRANSFER IN NAPHTHALENE-BASED COMPOUNDS AND DEVELOPMENT OF AN EFFICIENT HETEROGENEOUS CATALYTIC METHOD FOR THE AEROBIC C-H OXIDATION OF ALKYLARENES

By Eylül Çalıkyılmaz

September 2023

We certify that we have read this thesis and that in our opinion it is fully adequate, in scope and in quality, as a thesis for the degree of Master of Science.

Yunus Emre Türkmen

(advisor)

Halil İbrahim Okur

Çağatay Dengiz

Approved for the Graduate School of Engineering and Science:

Orhan Arıkan

Director of the Graduate School of Engineering and Science

ABSTRACT

INTRAMOLECULAR THROUGH-SPACE CHARGE-TRANSFER IN NAPHTHALENE-BASED COMPOUNDS AND DEVELOPMENT OF AN EFFICIENT HETEROGENEOUS CATALYTIC METHOD FOR THE AEROBIC C-H OXIDATION OF ALKYLARENES

Eylül ÇALIKYILMAZ

M.Sc. in Chemistry

Advisor: Yunus Emre Türkmen

September 2023

The transfer of electrons between two molecules or between different groups attached to a molecule is known as charge transfer. Electronic communication can take place either through chemical bonds or through space. Intramolecular through-space charge transfer occurs between donor and acceptor parts of a molecule depending on the electron density difference, the distance between them, and their relative positions. The main objective of the project is to study the phenomenon of intramolecular through-space charge transfer in naphthalene-based organic materials. We investigated the charge transfer in 1,8-substituted naphthalene derivatives and the effect of different electron-donating and electron-withdrawing groups. To investigate the role of these groups, a variety of control substrates which have different electronic structures were synthesized. Subsequently, it was

determined which substances possess a charge transfer band by examining the UV-Vis spectra of these substances. Additionally, it was found that substances with charge transfer bands in UV-Vis absorption spectroscopy had multiple emission values when fluorescence spectra were analyzed. In addition, to observe the effect of different solvents on charge transfer, the substance with observed charge transfer was dissolved in different solvents and examined in terms of color, absorption, and emission values.

A key objective of the second part is to develop an environmentally friendly and efficient earth-abundant metal hydroxide catalyst that can be used in aerobic C-H activation reactions for a variety of organic compounds. Metal hydroxides are used for this purpose because of their ability to operate at relatively low temperatures and it allows metal hydroxides to act as highly effective catalysts for oxidation reactions. As an earth-abundant metal-containing catalyst**,** $Fe_xMn_{(1-x)}(OH)_y$ has been prepared by the Özensoy research group with different elemental ratios. In addition, the concentration of NaOH was systematically investigated during the synthesis of the catalyst. The catalytic activities of all catalysts were studied in the aerobic oxidation of fluorene to fluorenone as a model reaction. The optimized conditions were used for the oxidation of diphenylmethane to benzophenone. Subsequently, diphenylmethanes functionalized with electron-donating and electron-withdrawing groups were synthesized, and the yields of oxidation reactions were determined. Finally, the results of the kinetic isotope effect experiment were combined with the yields of the previous experiments to shed light on the mechanism of oxidation.

Keywords: Through-space charge transfer, naphthalene-based compound, solvatochromism,

dual emission, earth-abundant, metal hydroxide catalyst, aerobic C-H activation, fluorene.

ÖZET

NAFTALİN TEMELLİ BİLEŞİKLERDE İNTRAMOLEKÜLER UZAY-İÇİ YÜK TRANSFERİ VE ALKİLARENLERİN AEROBİK C-H OKSİDASYONU İÇİN ETKİLİ BİR HETEROJEN KATALİTİK YÖNTEMİN GELİŞTİRİLMESİ

Eylül ÇALIKYILMAZ

Kimya Bölümü, Yüksek Lisans

Tez Danışmanı: Yunus Emre Türkmen

Eylül 2023

Elektronların iki molekül arasında veya bir moleküle bağlı farklı gruplar arasında transferi, yük transferi olarak bilinir. Elektronik iletişim, kimyasal bağlar yoluyla veya uzay yoluyla gerçekleşebilir. Elektron yoğunluğu farkına, aralarındaki mesafeye ve göreceli konumlarına bağlı olarak bir molekülün verici ve alıcı kısımları arasında molekül içi yük transferi gerçekleşir. Projedeki temel amaç, naftalin temelli organik malzemelerde molekül içi uzay yük transferi olgusunu ve electron çekici-verici grupların bu olguya etkisini incelemektir. Bu amaçla, farklı elektronik yapılara sahip çeşitli kontrol substratları sentezlendi. Daha sonra bu maddelerin UV-Vis spektrumları incelenerek hangi maddelerin yük transfer bandına sahip olduğu belirlendi. Ek olarak, UV-Vis soğurma spektrumlarında yük transferi olan maddelerin, floresans spektroskopide çoklu emisyon değerlerine sahip olduğu gözlemlendi. Ayrıca farklı çözücülerin yük transferine etkisini gözlemlemek için yük transferi gözlemlenen madde farklı çözücülerde çözülerek renk, soğurma ve emisyon değerleri

açısından incelendi.

İkinci kısmın temel amacı, çeşitli organik bileşikler için aerobik C-H aktivasyon tepkimelerinde kullanılabilecek çevre dostu ve verimli, toprakta bol miktarda bulunan elementlerden oluşan bir metal hidroksit katalizörü geliştirmektir. Metal hidroksitler, nispeten düşük sıcaklıklarda çalışabilmeleri nedeniyle bu amaçla kullanılmaktadır. Bu özellikleri sayesinde metal hidroksitler, oksidasyon reaksiyonları için oldukça etkili katalizörler olarak hareket edebilirler. Toprakta bol miktarda bulunan metal içeren bir katalizör olan $Fe_xMn_{(1-x)}(OH)_y$ katalizörü Özensoy araştırma grubu tarafından farklı element oranları ile hazırlanmıştır. Ayrıca, katalizörün sentezi sırasında NaOH konsantrasyonu da sistematik olarak araştırılmıştır. Tüm katalizörlerin katalitik aktiviteleri, model tepkime olarak florenin florenona aerobik oksidasyonunda incelenmiştir. Optimize edilmiş koşullar difenilmetanın benzofenona oksidasyonu için kullanılmıştır. Daha sonra, elektron veren ve çeken gruplarla işlevselleştirilmiş difenilmetanlar sentezlenmiş ve benzofenon türevlerine dönüşümünün verimi belirlenmiştir. Son olarak, kinetik izotop etkisi deneyinin sonuçları, önceki deneylerin verimleri ile birleştirilerek oksidasyon mekanizması belirlenmeye çalışılmıştır.

Anahtar kelimeler: Uzaydan yük transferi, naftalin temelli bileşikler, solvatokromizm, dual emisyon, toprakta bol bulunan metal, metal hidroksit katalizörü, aerobik C-H aktivasyonu, floren.

ACKNOWLEDGEMENT

First of all, I would like to thank my supervisor, Yunus Emre Türkmen. I want to thank him for teaching me how to be a real scientist during my 3 years in the research group, allowing me to make mistakes, and patiently waiting for me to learn and improve.

I want to thank Emrah Özensoy for mentoring me in the collaboration project. I thank my dear Beyca for working with me on this project. It has been a pleasure to work with you since the second year of college, and it will always be a pleasure to be friends with you.

I would like to thank Dilgam Ahmadli and Yeşim Şahin who taught me everything I learned from the moment I entered the laboratory and continue to help me with everything. One of my biggest thanks goes to my dear Suay, with whom I never stopped working, laughing, and having fun side by side on the tiny bench of a vast laboratory. Even if we work in the most equipped laboratory in the world, I promise you that we will create our big world by working in a tiny space. I would also like to thank Merve Temel, Badar Munir, and Umut Mert Karacaoğlu, who were always with me and made the work enjoyable.

Aygün Şahin, thank you for pushing me to write my thesis even when you were not physically with me and preventing me from leaving it until the last night, and for being the big sister I later found. Ekim Sevil, thank you for our unbreakable bond, even though we are on opposite sides of the world, and for your excellent friendship. I have been thanking my little sister Defne for the past three years. My

life is filled with color because of her.

My most enormous thanks go to my dear mother, who never lost faith in me for a minute when everyone, including myself, thought I would never make it; my father, who made me stand on my own feet with his mentorship; my brother Umut, who made my life so much better with his deep conversations, his endless support, his jokes and all the meaningless things we watched and ate.

Finally, I would like to thank Ali Göktuğ Attar, to whom I dedicate this thesis. It is an excellent chance for me to find my best friend and my greatest love in the same person. I am glad that you are here.

LIST OF ABBREVIATIONS

DCM	Dichloromethane
FTIR	Fourier-Transform Infrared
HRMS	High-Resolution Mass Spectrometry
TLC	Thin-Layer Chromatography
NMR	Nuclear Magnetic Resonance
UV-Vis	Ultraviolet
THF	Tetrahydrofuran
DMSO	Dimethyl sulfoxide

Table of Contents

LIST OF FIGURES

LIST OF SCHEMES and TABLES

LIST OF NMR DATA

CHAPTER 1

INTRAMOLECULAR THROUGH-SPACE CHARGE-TRANSFER IN NAPHTHALENE-BASED COMPOUNDS

INTRODUCTION

(a) Charge Transfer

Charge transfer is the charge movement from an electron-rich donor to an electron-poor acceptor. Substances with this property are used today, particularly in technology, as organic light-emitting diodes.[1] Charge transfer can take place between two parts of a molecule that differ in electron density through the bond connecting these groups, and this is called through-bond charge transfer.[2] An example of this is polyimide **(1)**, which contains a donor diaminophenyl fragment and an acceptor diimide fragment **(Figure 1)**.[3]

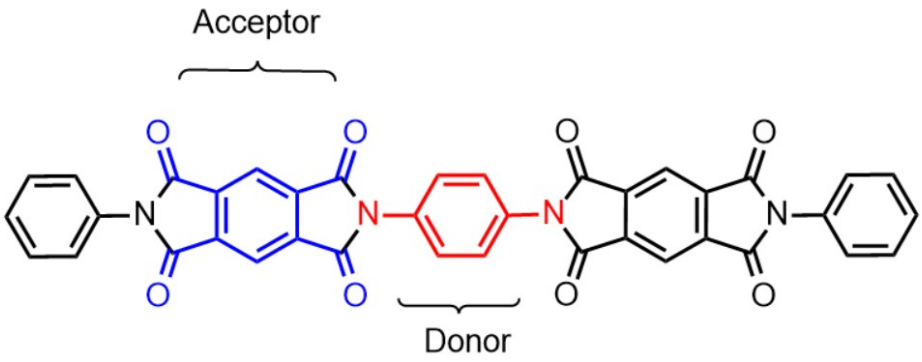

1

Figure 1: Through-bond charge transfer in polyimide derivative. [3]

Charge can also be transferred between two different molecules by passing through space, called intermolecular through-space charge transfer[4]. Charge transfer between[5] tetracyanoethylene and 1-chloronapthalene, and charge transfer between[6] 2,7-di(1-ethoxy 2-phosphonate) **(2)** and N,N'-diethylamine-NDI **(3)** are examples of intermolecular charge

transfer (**Figure 2**).

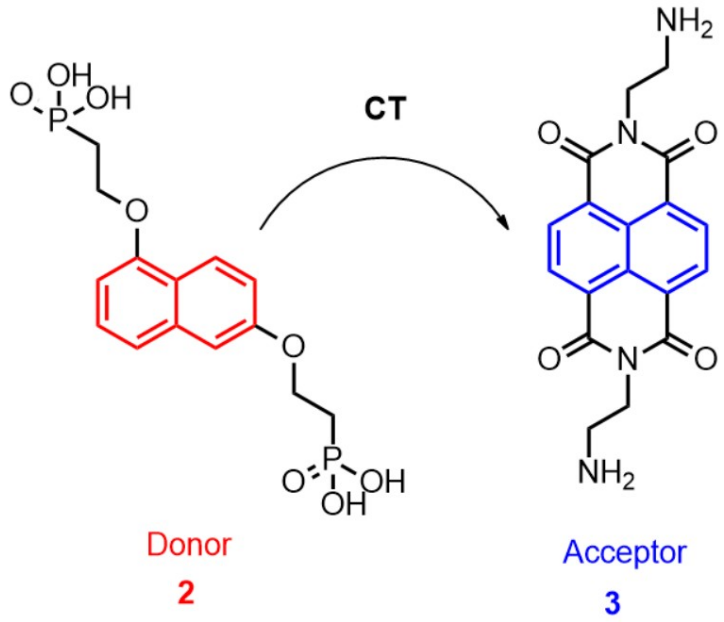

*Figure 2: Intermolecular charge transfer between compound **2** and **3**.*[6]

Charge transfer can also occur between two different parts of the same substance through the space. This phenomenon is known as intramolecular through-space charge transfer.[4]

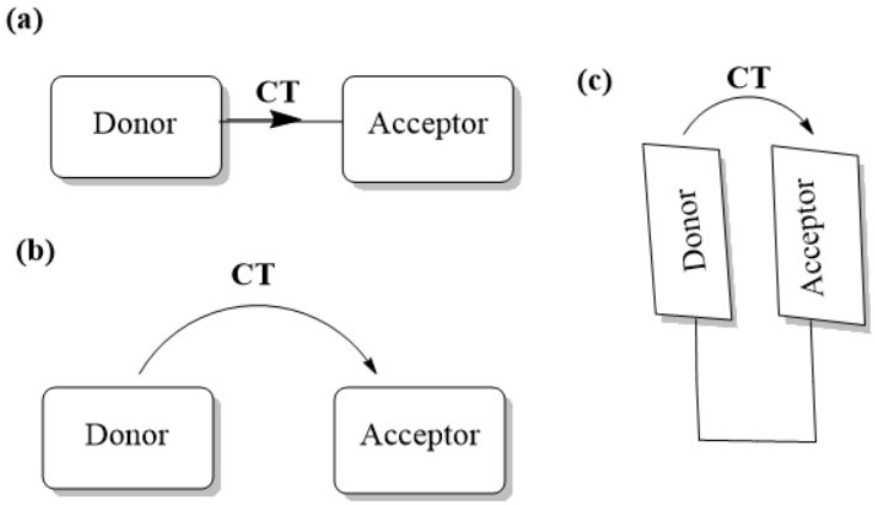

Figure 3: Representation of (a) Through- charge transfer, (b) Intermolecular through-space charge transfer, (c) Intramolecular through-space charge transfer.

(b) Intramolecular Through-Space Charge-Transfer

Intramolecular through-space charge transfer is the transfer of charge caused by the difference in electronic character between two different parts of a molecule.[1]

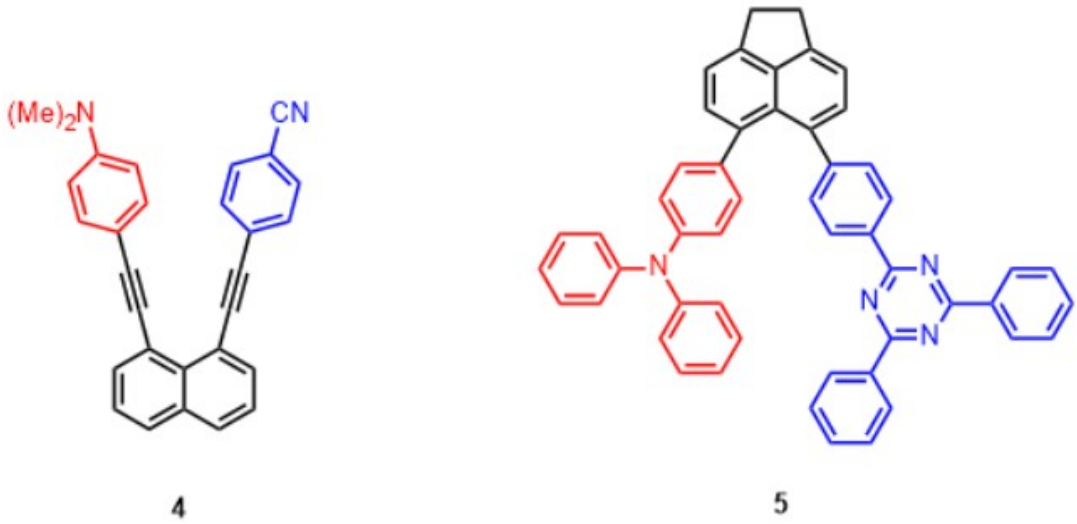

Figure 4: Intramolecular through-space charge transfer in naphthalene-based, U-type fluorophore derivative[7] and TPa-ace-TRZ.[8]

For this transfer to occur, the distances and positions of the electron donor and acceptor moieties relative to each other are important. The HOMO-LUMO energy difference should also be small, since the charge transfer is from the HOMO of the electron-rich group to the LUMO of the electron-poor group.[4] In the naphthalene-based, U-type fluorophore derivative[7] **4**, through-space charge transfer was observed due to the electronic difference created by the electron-withdrawing -CN and electron-donating $N(Me)_2$ groups in the phenyl rings and the relative orientation and distance of the phenyl rings. The same trend was also observed in the TPa-ace-TRZ compound **5 (Figure 4)** with charge transfer band around 350 nm.[8]

(c) Characterization of The Charge Transfer Complexes

The charge transfer character of a substance can be understood primarily by its physical appearance. Most charge-transfer complexes have an intense color.[9] The spectroscopic explanation for this color is as follows: Two different signals can be observed in the UV-Vis spectrum of a complex. The first is an absorption signal around 300 nm, which is due to the nature of the molecule, and the second is an extra red-shifted peak in the visible region, which is due to the charge transfer between donor and acceptor.[9] This peak can also be called the charge transfer band and the presence of this signal explains the intense color of the substance.[10] When Jara et al. recorded the UV-Vis spectrum of 5-[(4-dimethylaminophenyl)methylene] dye by dissolving it in water, they observed a peak around 500 nm in addition to the absorbance around 350 nm and identified this signal as charge transfer band.[11]

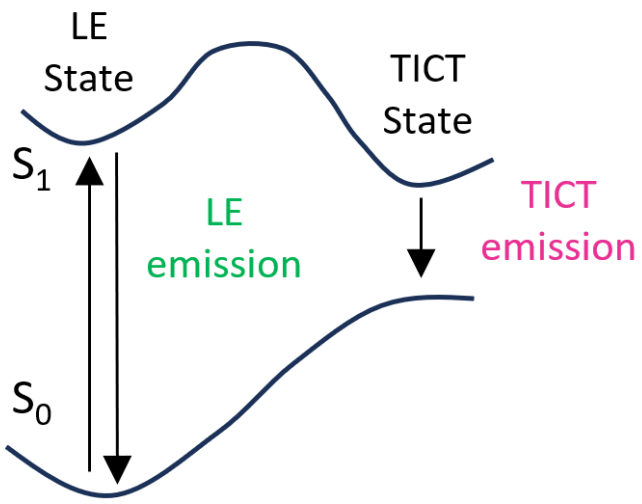

Figure 5: Emission path of a charge transfer compound.

A special feature of charge transfer complexes is also observed when they are analyzed by fluorescence spectroscopy.[12] These substances show double emission in their fluorescence spectra.[13] In fluorescence spectroscopy, the excited molecule emits at a

characteristic wavelength. However, in charge transfer complexes, dual emission is observed instead of single emission. Normally, electrons going from the ground state to the local excited state emit from here and this gives us the local emission (LE) signal. But in the charge-transfer complex, the emitted electrons can follow two different paths. First, emission can occur from the excited state. Secondly, the electrons in the excited state can go to the charge transfer state at a lower energy level and emit from twisted intramolecular charge transfer state. (TICT) (see **Figure 5**).[14]

(d) Solvatochromism

Solvatochromism is the observed change in the color of a solute depending on the solvent in which it is dissolved.[15] This phenomenon can be observed physically and analyzed by spectroscopic techniques. UV-Vis spectroscopy is commonly used to observe the solvatochromism effect. By UV-Vis spectroscopy, it is observed which wavelengths are absorbed by the substance. As mentioned above, since different colors are observed with different solvents in solvatochromism, an absorption signal at different wavelengths is expected in UV-Vis spectra.[16]

There is a chemical reason for this physically observed tendency to change color. The delocalization of electrons is a property that increases the stability of a substance. Conversely, the accumulation of electrons in one region causes a dipole moment and reduces the stability of the substance. Solvatochromism also works to increase stability by decreasing the current electron accumulation. The electronic ground state or excited state of a solution can have a higher dipole moment. Accordingly, the polar solvent will increase the stability of the state with more dipole moment.[17]

If the dipole moment in the excited state is higher, the polar solvent stabilizes and

lowers the energy of the excited state. This reduces the energy gap between the ground state and the excited state. A lower energy signal is therefore expected in the absorption and emission spectra. If the situation is reversed, the polar solvent stabilizes the ground state and reduces its energy, so that the gap between the excited and ground states becomes larger. In this case, on the contrary, a shift to higher energy, i.e. lower wavelength, is observed.[17]

(e) Marcus theory of electron transfer

The first thing to consider when looking at the solvent effect in electron transfer complexes is whether charge transfer or solvent stabilization of one of the states occurs first. According to the Libby theory of electron transfer, there should be an order between these two events. For charge transfer to occur, the groups are expected to move from the equilibrium state to a higher potential energy state, and then charge transfer is expected to occur. And only after the charge transfer has taken place can the solvent reorganize.[18] However, Marcus theory argues that such a high activation energy is not required to move from the equilibrium state to the charge transfer state.[19,20] According to this theory, a quarter of the activation energy mentioned in the Libby theory is sufficient for charge transfer to take place (see **Figure 6**). Therefore, internal reorganization and solvent reorganization occur simultaneously, not sequentially.[21] In this context, if solvent reorganization and charge transfer occur at the same time in terms of timing, it is expected to observe a result in accordance with the Marcus theory; if they do not occur at the same time, it is expected to observe a result in accordance with the Libby theory. In other words, in the Marcus theory condition, it is expected to observe a shift in the absorbance and fluorescence spectra in opposite directions depending on the solvent polarity. Laage et al

observe this result with charged pushed-pull polyenes.[17]

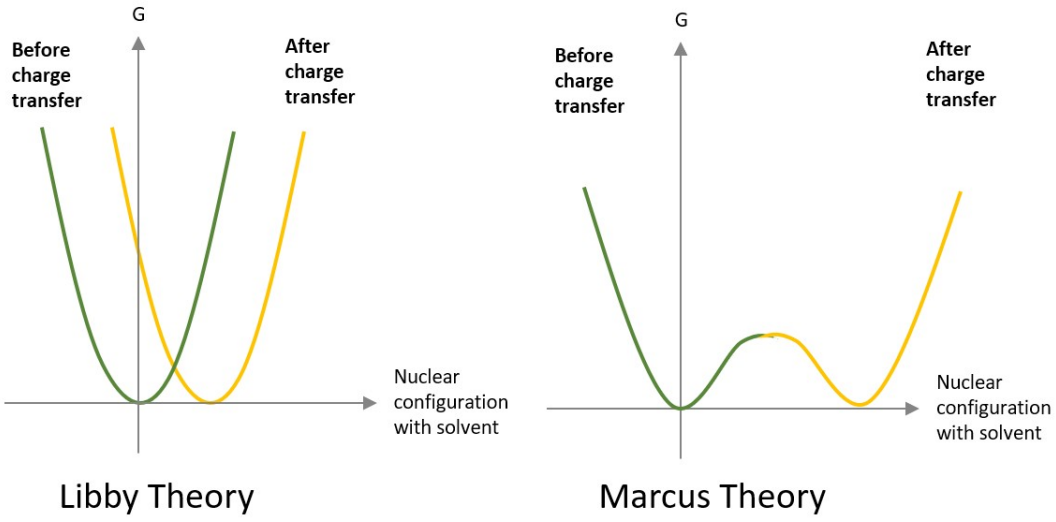

Figure 6: Scheme of Libby and Marcus theory.

THE AIM OF THE PROJECT

In the previous article we published for the synthesis of hydroxyfluoranthene derivatives,[22] the aim was to obtain fluoranthene derivatives in three steps. Firstly, 1,8-diiodonapthalene was reacted with alkynol using Sonogashira coupling. Then oxidation of alkynol derivative to alknone was carried out. Finally, the product obtained **6** was subjected to Suzuki-Miyaura coupling with furan-2-boronic acid. The main logic of the project came into play in this step. The electron rich furan and the electron poor alkynone group spontaneously entered an intramolecular Diels-Alder reaction and gave compound **8.** The

cyclic product formed afterwards was spontaneously opened to provide aromaticity again. In this way, the desired fluoranthene derivative **9** was obtained.

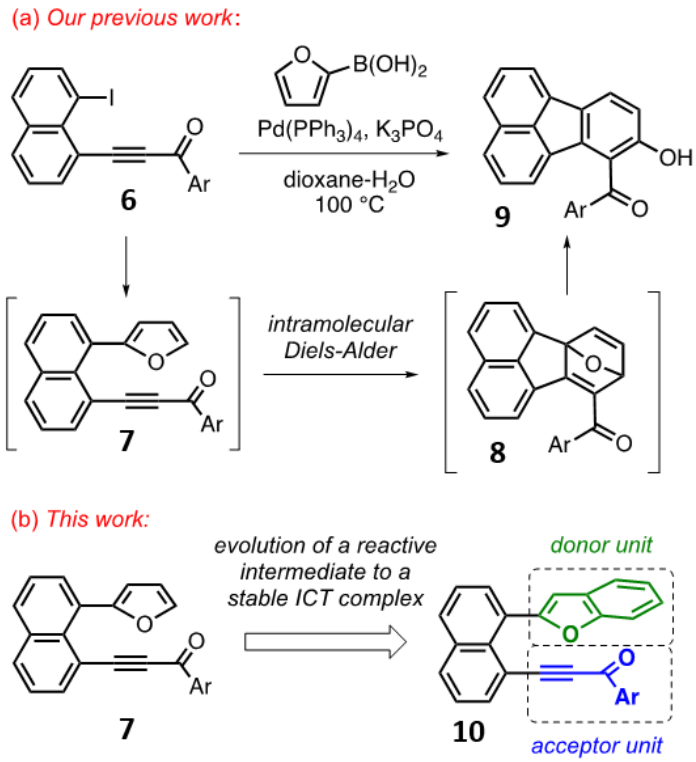

Scheme 1: General scheme of the previous work[22] and this work.

For the continuation of the project, the Suzuki-Miyaura coupling was tried again by changing the furan derivative and using benzo[b]furan-2-boronic acid. However, this time the only compound that could be isolated was the Suzuki product **(10a)**. This was not an

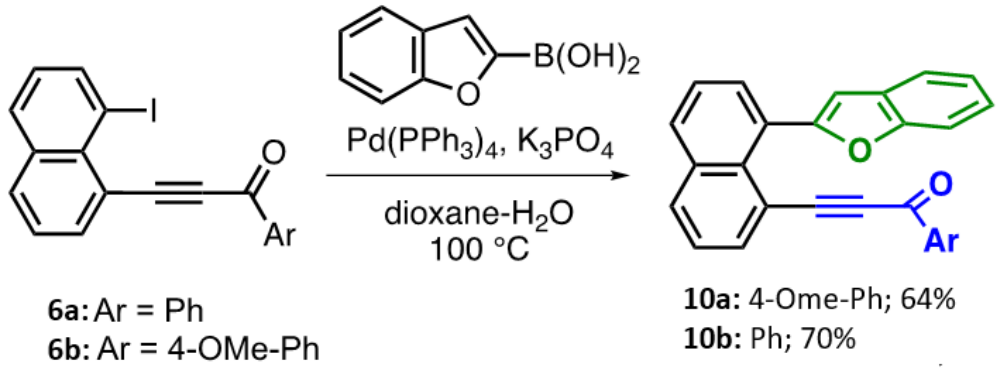

Scheme 2: Synthesis scheme of 10a and 10b.

product (**10a**) was intense red. Considering the electron donating and withdrawing groups attached to naphthalene, it was thought that intramolecular through-space charge transfer might be possible in **10a**. Therefore, it was decided to synthesize **10b** and to investigate whether **10a** and **10b** have intramolecular through-space charge transfer properties. After obtaining Suzuki product **10b** again, it was decided to try to obtain Diels-Alder reaction. To push the reaction to take place, the Suzuki product **(10b)** obtained was heated in chlorobenzene to 150 °C.[23] According to ^{1}H-NMR analysis, the substance did not undergo decomposition or Diels-Alder reaction, remaining as Suzuki product. However, an interesting result was also obtained.

The main aim of the project is to prove by UV-Vis absorption and fluorescence

spectroscopy that substances **10a** and **10b** fulfil the intramolecular through-space charge-transfer trend. To observe the effect of the functional group on the observed charge transfer, different control substrates **(11, 12, 13** and **6a)** were synthesized, and the same analyses were performed. Having observed no charge transfer in the control substrates, mixtures of **14** and **15** were analyzed to investigate intermolecular through space charge transfer, but no charge transfer was observed. Finally, to investigate the effect of solvent on charge transfer, the solution of **10a** in 6 different characteristic solvents was analyzed and an attempt was made to obtain a trend according to polarity of the solvents.

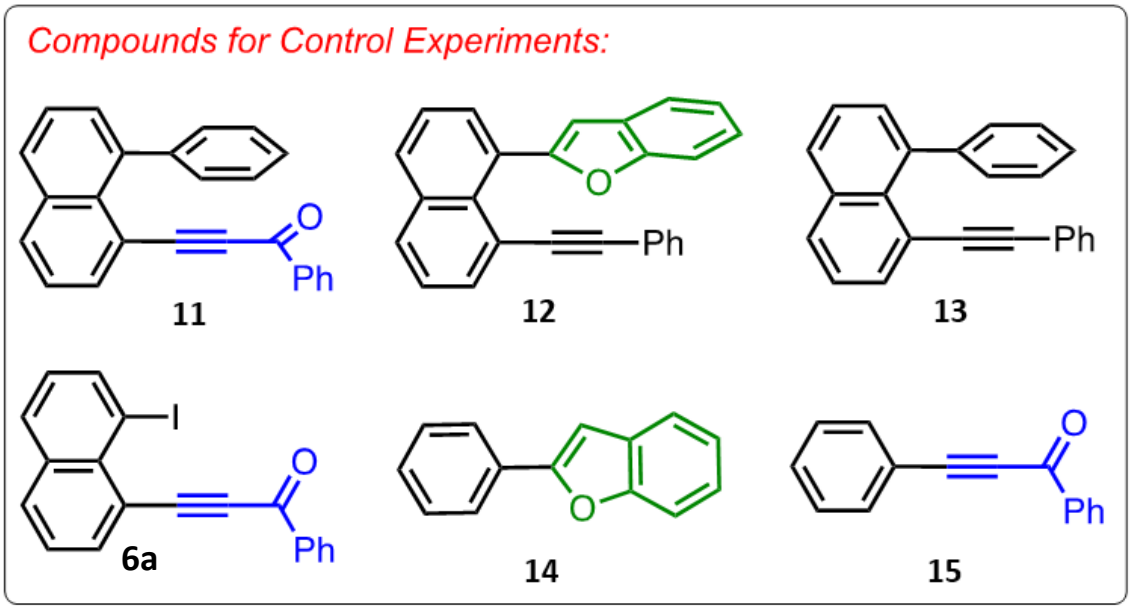

Figure 7: Molecular structures of the control substrates.

RESULTS AND DISCUSSION

(a) Discovery and analyses of the charge-transfer complexes

In the previous study, various fluoranthene derivatives were synthesized by Sonogashira and Suzuki-Miyaura coupling. The logic was to functionalize 1,8-diiodonapthalene with electron-rich furan and electron-poor alkyne to undergo a rapid intramolecular Diels-Alder reaction. This was followed by rapid ring opening to provide aromaticity (see **Figure 7**).[22]

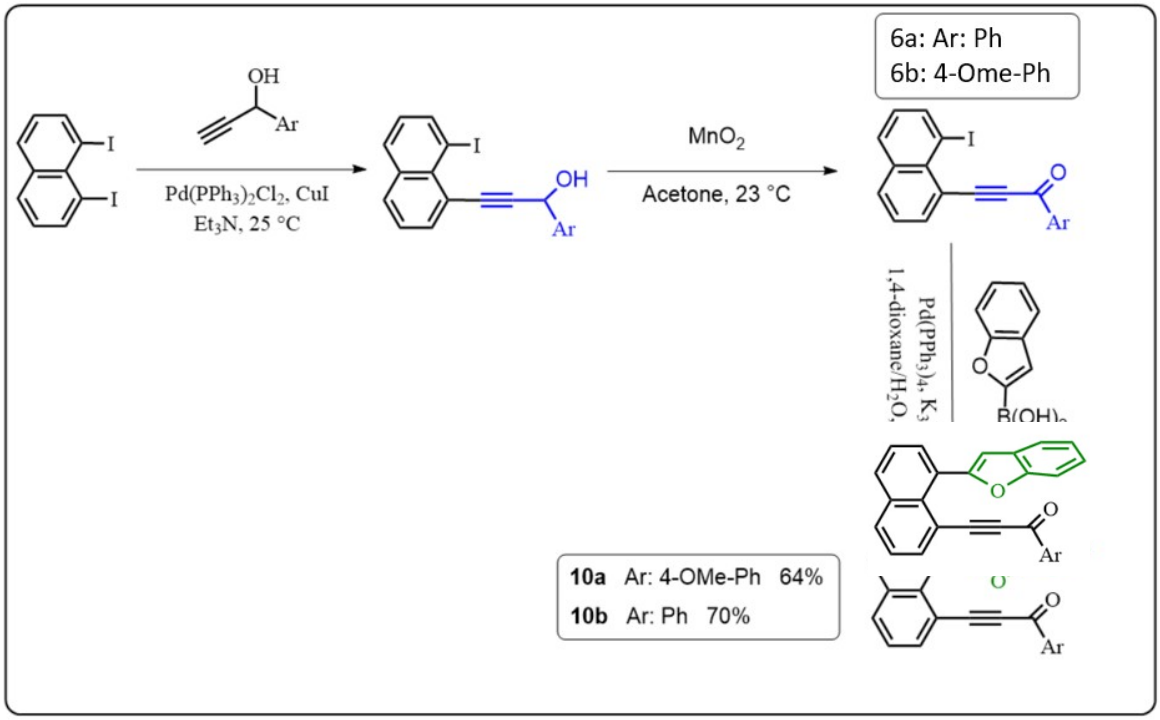

Scheme 3: The synthesis of compounds 6a, 6b, 10a and 10b.

To test the effect of the diene structure, substrate **10a** and **10b** was treated with benzo[b]furan-2-boronic acid instead of furan-2-boronic acid for Suzuki-Miyaura coupling (**Scheme 2**). Because aromaticity of both benzene and furan should be broken, the resulting

Figure 8: Photos of 10a and 10b under daylight sequentially.

Suzuki product **10a** and **10b** did not undergo the Diels-Alder reaction. The substrate **10b** is heated to 150 °C in chlorobenzene in the next step. However, according to the ^{1}H-NMR, the Diels-Alder reaction did not take place. The color of **10a** was observed as

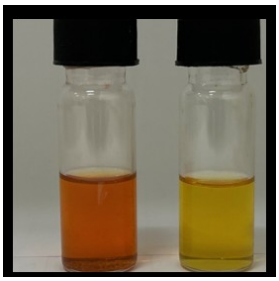

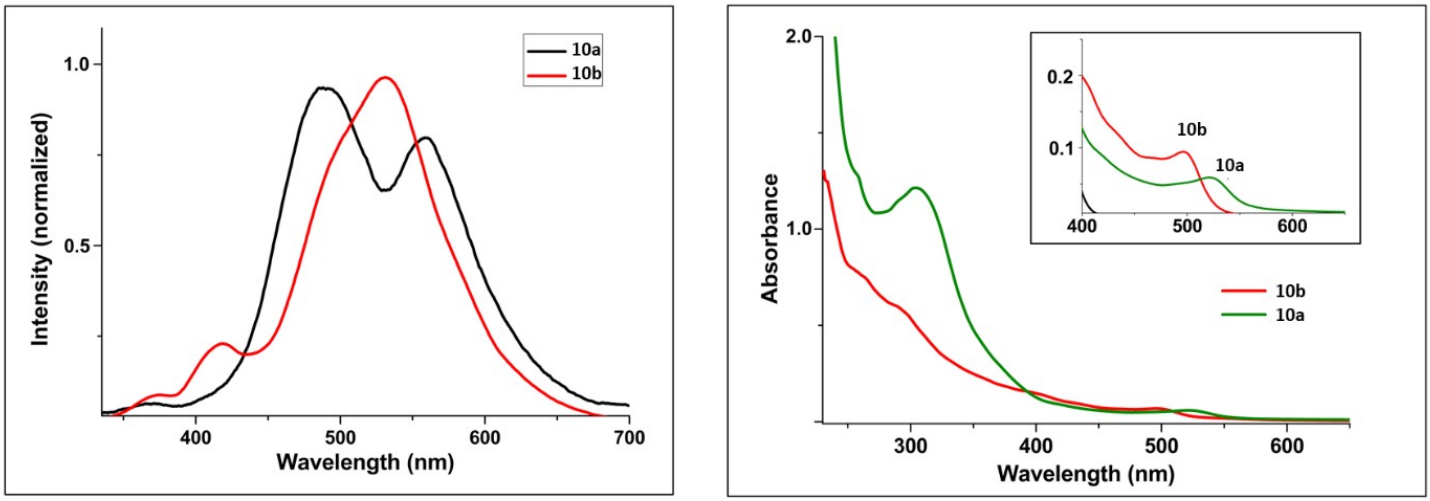

Figure 9: (a) UV-Vis spectrum of 10a and 10b, (b) Fluorescence spectrum of 10a and 10b. (in 2.5 x 10^{-5}M)

red and the color of **10b** was orange. This result, together with the presence of electron-rich and electron-poor moieties, led to the suggestion that there might be a charge transfer between the benzofuran moiety and the alkyne moiety of the substrate. Therefore, the UV-Vis absorption spectrum (**Figure 9a**) of **10a** and **10b** was recorded to test this hypothesis. It was seen that, there is a charge transfer band at **526 nm** for **10a** and **500 nm** for **10b.** Then, the fluorescence spectrum was evaluated **(Figure 10b)**, and the observed dual emission (**410 nm**, **532 nm** for **10a**; **493 nm**, **560 nm** for **10b**) strongly support that there is an intramolecular through-space charge transfer in compounds **10a** and **10b**.

(b) Synthesis and Analysis of Control Substrates

By using Suzuki-Miyaura and Sonogashira coupling procedures[22], test compounds **11, 12, 13, 6a, 14** and **15** were synthesized (**Scheme 4**) to prove that charge transfer occurs due to the electronic structure of the functional groups on naphthalene. This was done to maintain one acceptor or donor functional group while replacing the other with a group with a different electronic structure each time. Because the naphthalene skeleton remains the same, the distance between functional groups and their position relative to each other would not change, but the difference in electron density would. All the test substances were investigated by UV-Vis and fluorescence spectroscopy (**Figure 10**). No charge transfer band was observed in the UV-Vis spectrum of any test substance.

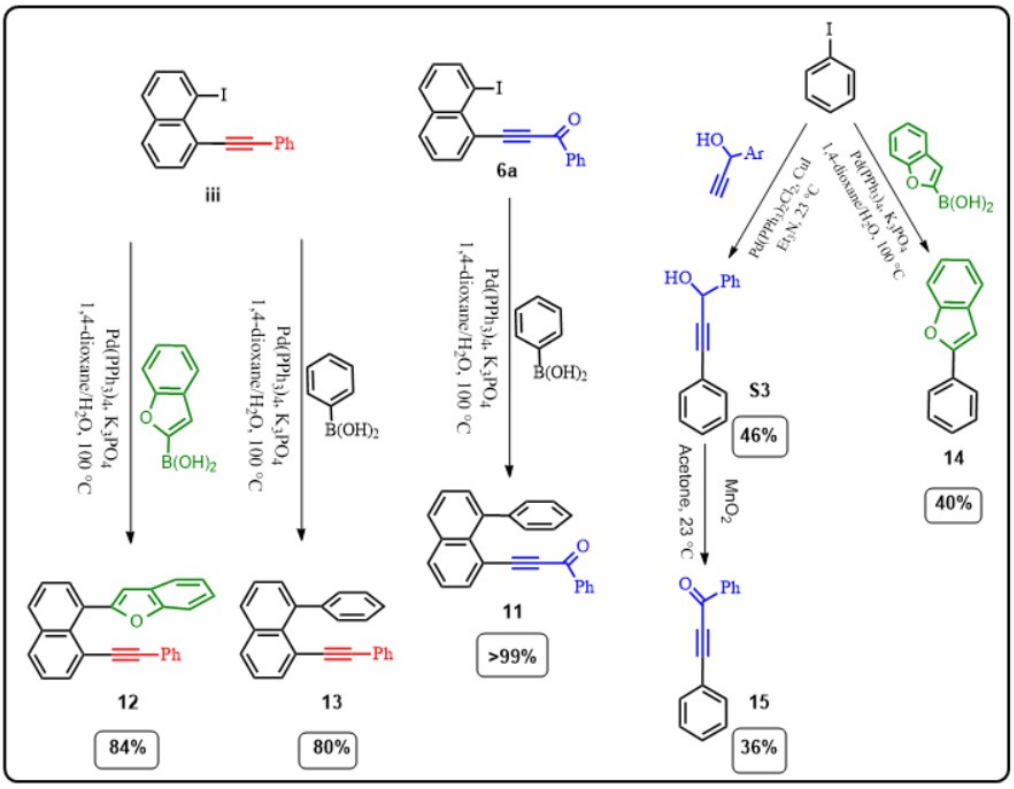

Scheme 4: Synthesis scheme of control substrates.

Substances **14** and **15** were obtained by attaching the functional groups of the substance with observed charge transfer to iodobenzene. It was done to see if charge transfer could be observed in the solution prepared by mixing substances **14** and **15**. Despite not being

connected to the same substrate, the electron donor and acceptor groups would still be in contact in the solution. To test the hypothesis, absorption data was collected with four different concentrations of the mixture of **14** and **15**. To have a higher interaction between **14** and **15**, 1.0 10^{-2} M solution of mixture was prepared. Even with that concentration, no charge transfer band was observed in UV-Vis spectrum (**Figure 10c**). It shows that for substrates **10a** and **10b**, intramolecular charge transfer can occur in even at very low concentrations while intermolecular charge transfer cannot be observed in relatively higher concentration. This result could be accommodated to the effective molarity of the charge

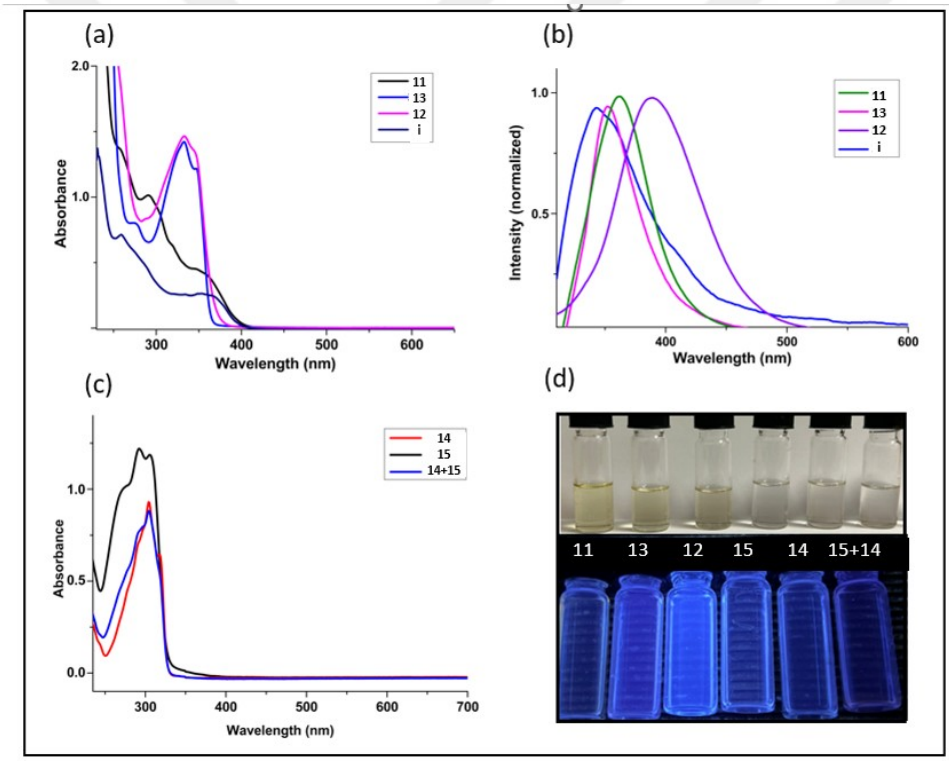

Figure 10: (a) Absorbance spectra of 3a, 3b, 3c and 3d in DCM (b) emission spectra of 11, 12, 13, i in DCM, (c) Absorbance spectra of 14 and 15 mixture of 14-15, (d) photo of 11, 12, 13, 14, 15 and mixture of 14-15 (top: under daylight bottom: under 366 nm.

Comp.	Absorbance		Emission (nm)
	$\times_{max}$ (nm)	CT (nm)	
10a	306	526	493, 560
10b	289, 399[a]	500	410, 532
11	290, 344	-	404
13	332, 347	-	379
12	333	-	423
6a	352	-	402

Table 1: Absorbance and emission values of **10a, 10b, 11, 12, 13** and **6a**

(c) Solvatochromism with 10a

To test the solvatochromism trend, absorbance and emission spectra were recorded with 6 different solvents using substance **10a**. It was expected that absorbance and emission would show a red or blue shift as the polarity of the solvent increased. This would vary depending on which of the ground or excited states had a higher dipole moment. For example, if the dipole moment of the excited state was higher, the more polar solvent would stabilize the ground state, causing a red shift. But whatever the conditions, emission and absorbance were expected to follow the same trend. However, the observed results were different from the classical solvatochromism results. As the solvent polarity increased, the

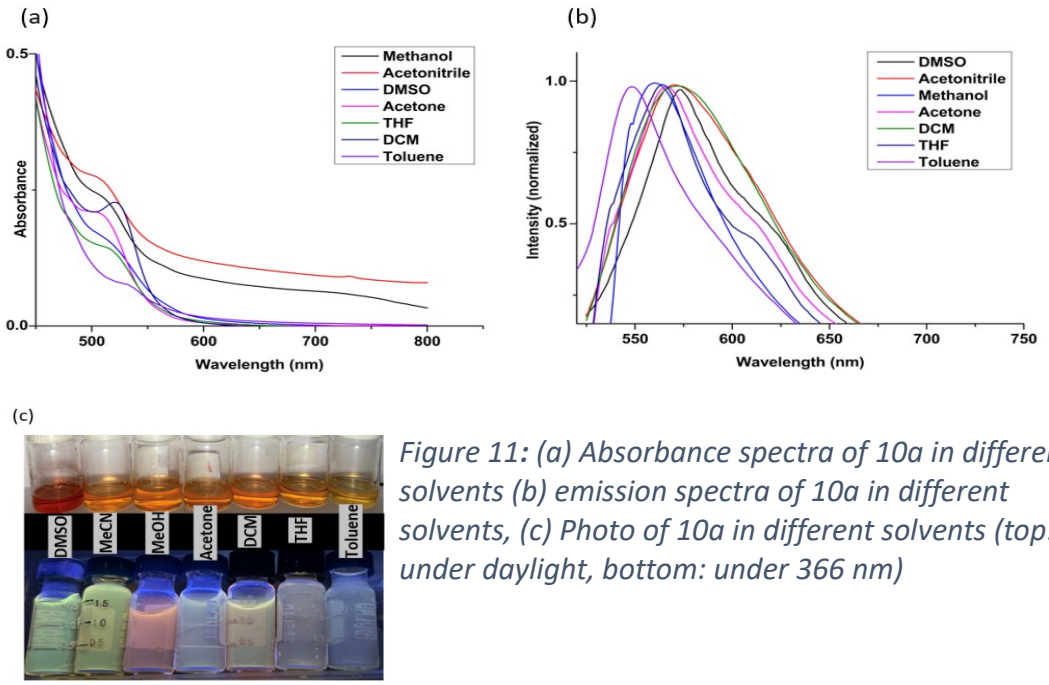

Figure 11: (a) Absorbance spectra of 10a in different solvents (b) emission spectra of 10a in different solvents, (c) Photo of 10a in different solvents (top: under daylight, bottom: under 366 nm)

absorbance values

showed a blue shift, but the emission values showed a red shift (see **Figure 11**). Toluene, the most nonpolar of the seven solvents, has the highest λ_{max} value for absorption (**533 nm**) and the lowest λ_{max} value for emission (**550 nm**). DMSO, the most polar solvent, gives the lowest λ_{max} value in absorption (**509 nm**) and the highest in emission (**573 nm**) (see **Table 1**).

Laage et al. suggest that a similar situation may exist due to charge transfer.[17] According to the way solvatochormism is usually defined, it is known that the solvent changes the electronic configuration of the ground state and therefore a shift is observed according to the solvent polarity and the dipole moment of the excited state. [24]

However, due to the charge transfer from the ground state to the excited state, the solvent orientation in equilibrium with the ground state is not in equilibrium with the charge distribution in the Franck-Condon excited state. Therefore, the absorbance and emission transition energies must be defined as a function of different factors. The absorbance transition energy is the sum of the adiabatic energy difference between the ground and excited states and the solvent rearrangement energy of the excited state. On the other hand, the emission energy is calculated by subtracting the solvent reorganized ground state energy from the above difference (adiabatic ground and excited state energy difference). Given this information when the effect of solvent polarity is analyzed:

1. A more polar solvent will increase the energy of both solvent reorganized states (ground and excited), but this effect will lead to an increase in the absorbance transition energy and a decrease in the emission transition energy.

2. Since the reorganization free energy is the difference between the two solvent states, the difference will remain almost constant even if the solvent is changed.

This means that a blue shift in the absorbance spectra and a red shift in the emission spectra would be expected, as observed.[17,25]

However, an interesting trend emerges when analyzing combinations of emission and absorption energies rather than looking at them separately. The wavenumber averages for all solvents are almost the same. This is called symmetrical solvatochromism and is explained by the Marcus theorem. Because solvent reorganization and internal reorganization (charge transfer) occur simultaneously, the solvent polarity shows a different trend than most substances.[25]

$\tilde{\nu}$	**Absorption - λ_{max} (nm)**	**Emission - λ_{max} (nm)**	(cm^{-1})	(cm^{-1}) $\tilde{\nu}$	**Average** (cm^{-1})
DMSO	509	573	0.0020	0.0017	0.0019
Acetonitrile	513	571	0.0019	0.0018	0.0019
Methanol	509	571	0.0020	0.0018	0.0019
Acetone	508	566	0.0020	0.0018	0.0019
DCM	521	560	0.0019	0.0018	0.0019
THF	517	564	0.0019	0.0018	0.0019
Toluene	533	550	0.0019	0.0018	0.0019

*Table 2: λ_{max} values for **10a** in different solvents (wavenumber is directly proportional to the energy).*

CONCLUSION

In summary, naphthalene-based complexes (**10a** and **10b**), which are electron-donating benzofuran and electron-deficient alkynone groups at positions 1 and 8, were synthesized using 1,8-diiodonaphthalene as the skeleton. The intense red color of **10a** and the intense orange color of **10b** suggest that they behave as donor-acceptor due to the electronic properties, relative positions, and proximity of the two functional groups. The analyses revealed an intramolecular through-space charge transfer in the complexes. In the results obtained from the UV-Vis spectrum, the charge transfer band was observed at **526 nm** additional to the absorbance band at **306 nm** belonging to the substance. The fluorescence spectrum of the compound was analyzed, it was found that there was double emission due to charge transfer. Control substrates were synthesized by keeping one of the functional groups constant and changing the other each time, and it was found that they did not exhibit the expected charge transfer property. In order to prove that the charge transfer tendency was due to the electronic property only, iodobenzene was functionalized with donor-acceptor functional groups. No charge transfer was observed in the analyses of the 10^{-2} M solution of the mixture of these two benzene derivatives. Finally, the solvatochromism experiment with substance **10a** gave a result that excluded the classical definition of solvatochromism. With increasing solvent polarity, a blue shift in absorption and a red shift in emission were observed.

CHAPTER 2

DEVELOPMENT OF AN EFFICIENT HETEROGENEOUS CATALYTIC METHOD FOR THE AEROBIC C-H OXIDATION OF ALKYLARENES

INTRODUCTION

(a) C-H Activation

C-H activation is a key functionalization step in most chemical syntheses.[26,27] Thanks to the cleavage of carbon and hydrogen bonds, the new bonds that carbon can form with other atoms play an important role in the synthesis of more complex molecules. Selective functionalization requires precious metal catalysts, which in classical methods are used at high temperatures and in large quantities.[28] Alternatively, C-H activation can be carried out in several steps using the directing group effect. However, if we combine C-H activation with green chemistry, the aim is to develop an environmentally friendly method by performing a stepwise synthesis that uses fewer chemicals and generates less waste. To achieve this, it is very important to carry out this activation under mild conditions, with the least environmentally harmful substances, in as few steps as possible.[26]

(b) Earth-abundant Metals

Precious transition metals such as palladium and platinum used for C-H activation are effective in the reaction, but they also have many disadvantages. These metals are used in reactions that do not serve green chemistry because they are expensive, harmful to the environment and not readily available. For this reason, in recent years "earth-abundant metals" have been used, which are easily found in nature, cheap and environmentally

friendly.[29] There are many examples in the literature of the use of Earth abundant metals as catalysts. Some of the examples are the use of $FeCl_2$ as catalyst in the reaction using 2,3-dichloro-5,6-dicyano-1,4-benzoquinone oxidant for the activation of benzylic C-H bond[29] and the use of [NiFe]-LDH (Layered Double Hydroxide) nanosheet for water oxidation reaction.[30]

(c) Aerobic C-H Oxidation

Converting hydrocarbons into compounds such as alcohols, ketones, and carboxylic acids by selective oxidation is essential in the chemical industry because they can be used as building blocks of polymers, surfactants, or solvents.[31] To carry out this type of oxidation selectively, environmentally unfriendly substances such as HNO_3 ,[32] CrO_3, [33] or peracid[34] are used in the literature. However, to make this process environmentally friendly, the use of molecular oxygen as a stoichiometric oxidant has become widespread. This oxidation is called aerobic C-H oxidation.[35]

In the aerobic C-H oxidation reaction, in addition to molecular oxygen, metal oxide catalysts, metal-organic frameworks, and metal complexes are used. Although catalysts can be reused in these methods, the high temperature, high oxygen pressure requirement, or the necessity to use additives impose limitations on high yield, selectivity, and substrate scope.[35] The oxidation of *p*-xylene (**16**) to terephthalic acid (**17**) in the presence of cobalt, manganese salt and the radical initiator Br^- is an example of an aerobic C-H oxidation reaction **(Figure 12)**.[36]

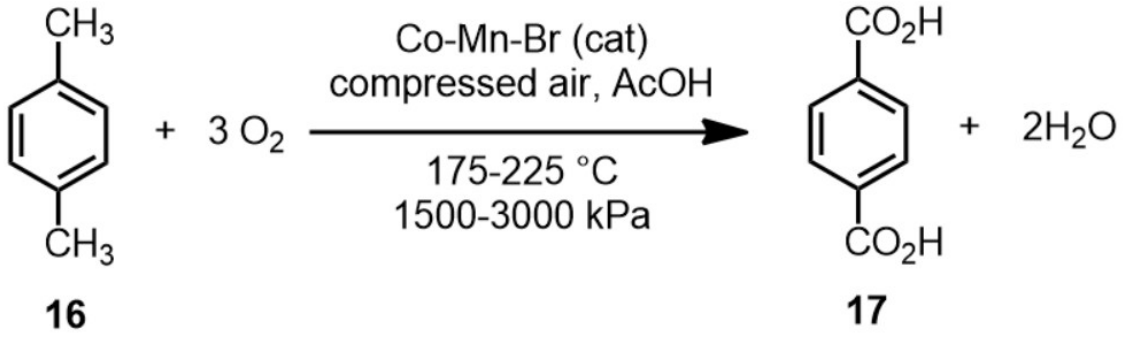

Figure 12: Aerobic C-H oxidation of p-xylene to terephthalic acid.[36]

(d) Layered Double Hydroxides (LDHs)

Layered double hydroxides are anionic clays containing two-dimensional, positively charged host layers and anions between these layers.[37,38] These structures can be used as heterogeneous catalysts for selective C-H activation in mild conditions. The two different metals in the host layers usually have one +2 and one +3 oxidation state. These two metals are uniformly distributed on the layer. Due to the uniform conveyance of positive charges on the LDH layers, electrostatic intuitive between the host and guest encourage the dispersion and stability of interlayer species. At the same time, the large surface area of LDHs plays an important role in their catalytic function.[38]

(e) Previous Studies about LDHs as catalyst for C-H oxidation

In the paper published in 2022 as a collaborative project between the Türkmen and Özensoy research groups, an earth-abundant LDH catalyst was used in C-H oxidation reactions.[39] The LDH catalyst used in this work, $Ni_xMn_{(1-x)}(OH)_y$, was used in the oxidation reaction of certain alkylarenes and alcohols. The main objective of this published work was to optimize the elemental ratios of the metals and the hydroxide concentration in the catalyst in order to determine the best performing catalyst in oxidation reactions. Once the

(a)

catalyst has been optimized as $Ni_{0.6}Mn_{0.4}(OH)_y$ the reaction mechanism was identified through

(b)

mechanistic studies. Sika-Nartey et al. followed the following path to determine the mechanism. The reaction from fluorene (**18**) to fluorenone (**19**) was carried out in an inert atmosphere without oxygen. As a result of this reaction, a dimerization (**20**) yield of 3% is obtained, while a low yield of 11% of fluorenone (**19**) is obtained.

Scheme 5: (a) Fluorene oxidation with molecular oxygen, (b) Fluorene oxidation in inert atmosphere.[39]

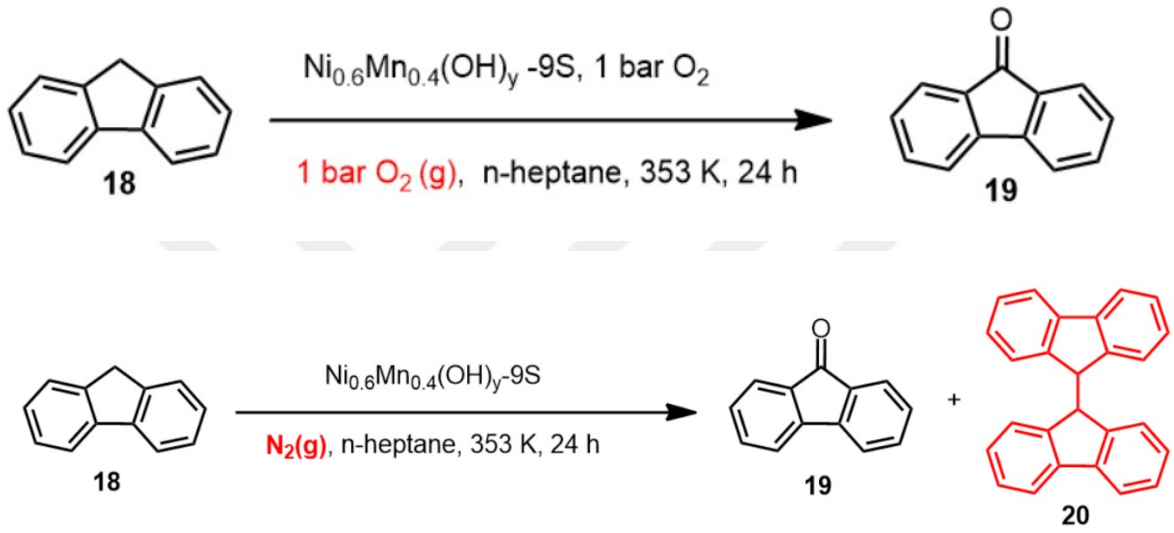

(f) Kinetic Isotope Effect

The kinetic isotope effect is found by replacing an atom in the reactant with one of its isotopes to find the mechanism of a reaction and analyzing the result using techniques such as NMR and MS. The technique is based on observing how the rate of a reaction changes

when there is a heavier isotope of the atom in the reactant. If we take the C-H oxidation reaction of fluorene **18**, benzylic protons are replaced by a heavier isotope, deuterium. Because deuterium is heavier than hydrogen, its vibrational energy is lower, and a slowdown is expected when deuterium is involved in the rate-determining step.[41] When the C-H bond cleavage rates of these two substances are compared, if the one with deuterium shows a slowdown, it is understood that it is the rate-determining step in C-H cleavage.[40] The kinetic isotope effect for this reaction is calculated as k_{C-H}/k_{C-D}. This calculation can be made using ^{1}H NMR as follows:

Consider the case of fluorene: When deuterated fluorene and fluorene are mixed 1:1 (0.25 mmol of each) and reacted, the kinetic isotope effect can be calculated by NMR analysis of the resulting mixture as follows. The benzylic protons of fluorene are expected to singlet at around 3.9 ppm. At 7.85 ppm, the aromatic proton signal from both fluorene and deuterate fluorene represents 4 protons. Finally, the aromatic proton signal from fluorenone around 7.7 ppm will again represent 4 protons. Considering that there are x mmol of fluorene and x mmol of deterred fluorene at the beginning, the two benzylic protons at 3.9 represents the unreacted part of fluorene. Since the other two aromatic signals will be common to deuterated fluorene and fluorene, one will indicate the unreacted part of deuterated fluorene and one will indicate the fluorenone formed. The ratio of the intensities of these three signals gives the kinetic isotope effect.[42]

THE AIM OF THE PROJECT

A new metal hydroxide catalyst, $Fe_xMn_{1-x}(OH)_y$, was synthesized based on the collaboration work of the Türkmen and Özensoy groups mentioned in the previous section.[39] The reason for using iron instead of nickel metal in this project is that iron is cheaper and its natural abundance is higher.[43] There are also more oxidation steps in iron than in nickel. Nickel tends to be in the +2 state, while iron tends to be in the +2 and +3 states, as well as +4, +5 and +6 states. Thus, iron's rich redox properties contribute to its synergistic properties.[44] All the synthesized catalysts with the same elemental ratios were tested in the fluorene oxidation reaction under the same conditions. Afterward, the catalyst optimization was completed by changing the NaOH concentration used during the synthesis. According to the results obtained, $Fe_{0.6}Mn_{0.4}(OH)_y$ was found to be the best working catalyst.

In the next step, the reaction conditions for the oxidation reaction of fluorene were optimized. All the conversion data were determined by using ^{1}H-NMR spectroscopy. After the conditions were also optimized for the oxidation of diphenylmethane, mechanistic studies were performed. An electronic property-conversion value correlation and kinetic isotope effect calculation were used to propose a catalytic reaction mechanism. The aim was to create a broad substrate scope for the oxidation of functionalized alkylrenes. In the part of the project included in this thesis, the effect of electron-donating and withdrawing groups on the conversion was investigated. The next step will be to expand the substrate scope and synthesize heteroatom-containing symmetrical and unsymmetrical diarylmethanes and show that the optimized conditions and optimized catalyst work in a broad spectrum.

RESULTS AND DISCUSSION

(a) Optimization of $Fe_xMn_{(1-x)}(OH)_y$ catalyst

To optimize the catalyst for aerobic C-H oxidation of alkyarenes, fluorene (**18**) oxidation to fluorenone (**19**) was used as sample reaction. The element ratio, precursor type and NaOH concentration used in the catalyst synthesis were varied while keeping other parameters constant. Each catalyst synthesized in this way was subjected to an oxidation reaction with fluorene (**18**) under the same conditions. Optimized catalysts were obtained according to the conversion data obtained by ^{1}H-NMR analysis. All the catalysts used in this work were synthesized by Beyzanur Erdivan from the Özensoy research group.

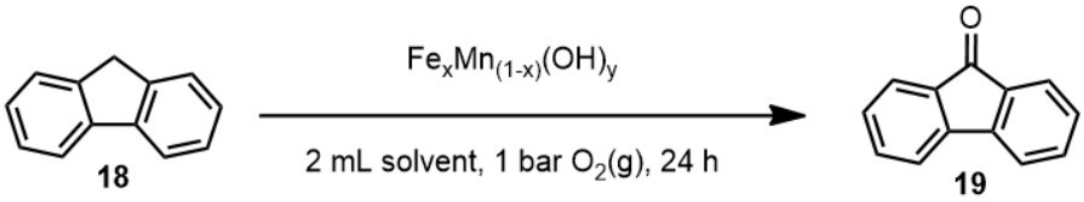

Scheme 6: General reaction scheme for oxidation of fluorene to fluorenone.

Before starting the experiments, it was necessary to ensure the purity of the fluorene to be used for the optimization. As the color of the fluorene purchased was off-white, as opposed to what it should be, recrystallisation was carried out using EtOH. After this process,

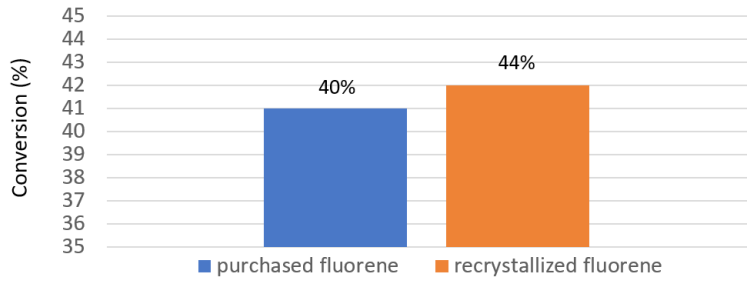

Figure 13: Oxidation conversion values for purchased fluorene and recrystallized fluorene.

(i) Elemental Ratio Optimization:

First of all, 11 different catalysts were synthesized with different elemental ratios of Fe and Mn. Two experiments were set up for each of the 11 catalysts to ensure reproducibility. During these experiments, the amount of fluorene, the temperature and the experimental time were kept constant.

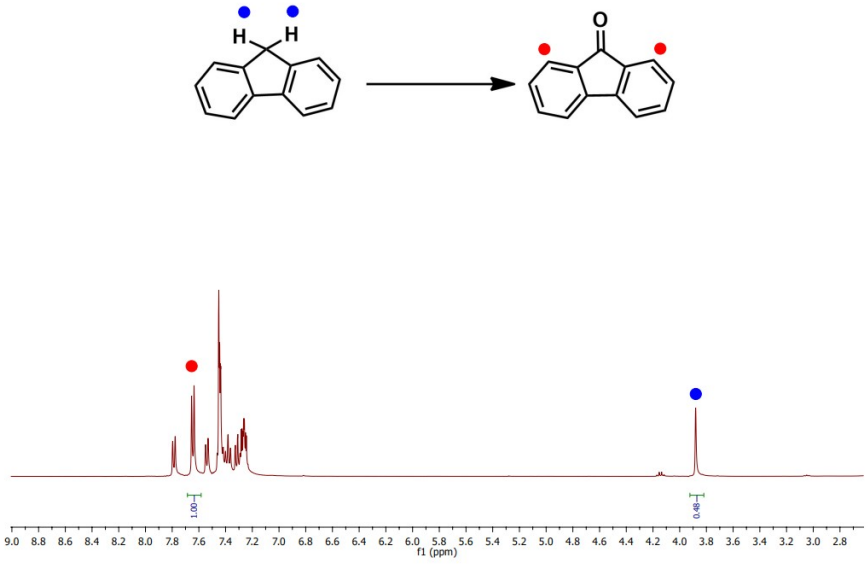

Figure 14: Sample [1]H-NMR spectrum of fluorene to fluorenone conversion.

[1]H-NMR spectroscopic analysis was then performed, and the percentage conversion was calculated. The key signals of fluorene and fluorenone were selected for this calculation. Two aliphatic protons at 3.87 ppm were selected for fluorene and two aromatic hydrogen protons at 7.62 ppm were selected for fluorenone. As both signals contain two protons, the calculation was performed as 1:1. In other words, if the integration values of the two signals are equal, this corresponds to a 50% conversion. (See **Figure 14**)

10 mg catalyst (x12S), 0.5 mmol fluorene, 80°C				
Catalyst	% Conversion 1	% Conversion 2	% Average	Variance
$Fe(OH)_3$	10	19	14,5	40,5
$Fe_{0.1}Mn_{0.9}(OH)_y$	44	42	43	2
$Fe_{0.2}Mn_{0.8}(OH)_y$	57	57	57	0
$Fe_{0.3}Mn_{0.7}(OH)_y$	60	60	60	0
$Fe_{0.4}Mn_{0.6}(OH)_y$	49	42	45,5	24,5
$Fe_{0.5}Mn_{0.5}(OH)_y$	68	65	66,5	4,5
$Fe_{0.6}Mn_{0.4}(OH)_y$	75	71	73	8
$Fe_{0.7}Mn_{0.3}(OH)_y$	56	53	54,5	4,5
$Fe_{0.8}Mn_{0.2}(OH)_y$	54	49	51,5	12,5
$Fe_{0.9}Mn_{0.1}(OH)_y$	26	28	27	2
$Mn(OH)_2$	7	9	8	2

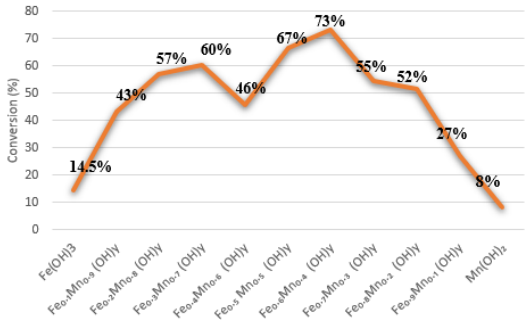

Figure 15: Elemental ratio optimization conversion data for fluorene.

The calculated average conversions indicated that the best performing catalyst was $Fe_{0.6}Mn_{0.4}(OH)_y$. Following this result, 6 additional catalysts were synthesized by varying the amount of NaOH used in the catalyst synthesis while keeping the elemental ratio constant.

(ii) NaOH concentration Optimization:

Since the catalyst is a hydroxide catalyst, changing the amount of NaOH also affects the -OH concentration. The effect of this concentration and the effect of the amount of sodium remaining on the surface after synthesis on the oxidation reaction was investigated by Özensoy Group. Again, as a result of the experiments carried out by keeping the reaction conditions constant, it was found that the best performing catalyst was the catalyst using 24.7 M (x12S) NaOH during synthesis. Note that 15 S represents the concentration at which NaOH reaches saturation in pure water, at 293 K. It corresponds to 1.26 g NaOH in pure water.[39]

(a)

$Fe_{0.6}Mn_{0.4}$ (OH), 6 wash NO3 precursor, 83.12mg fluorene				
	%Conversion 1	%Conversion 2	Average %	Variance
x1S	41	46	43,5	12,5
x3S	62	58	60	8
x6S	70	63	66,5	24,5
x9S	65	68	66,5	4,5
x12S	75	71	73	8
x15S	56	42	49	98

(b)

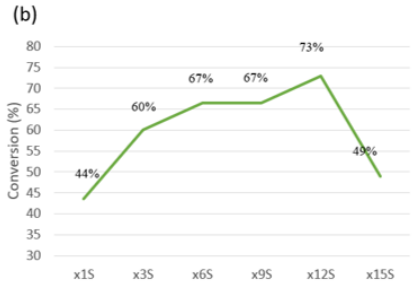

Figure 16: NaOH concentration optimization for $Fe_{0.6}Mn_{0.4}(OH)_y$ with fluorene oxidation.

(b) Reaction Condition Optimization for Fluorene:

Following the catalyst optimization, the reaction conditions were optimized. Experiments were carried out by varying the temperature and the amount of catalyst. As a result of the experiments, it was seen that a value close to full conversion was achieved at 90 °C using 15 mg of catalyst for oxidation of 0.5 mmol of fluorene.

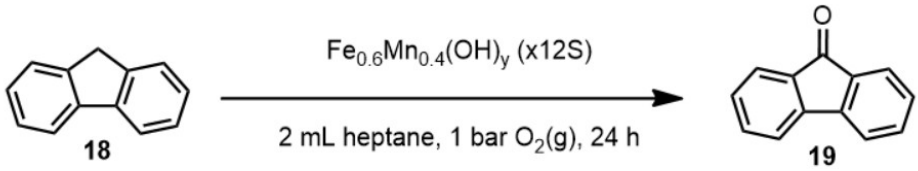

Scheme 7: Optimization of reaction conditions for oxidation of fluorene to fluorenone.

$Fe_{0.6}Mn_{0.4}(OH)_y$ x12S, 2 mL heptane 0.5mmol fluorene				
Catalyst	**% conversion 1**	**% conversion 2**	**Average % conversion**	**Varience**
10 mg catalyst, 80 °C	75	70	72,5	12,5
15 mg catalyst, 80 °C	94	91	92,5	4,5
15 mg catalyst, 90 °C	97	99	98	2

Table 3: Optimization of Reaction conditions for fluorene oxidation.

(c) Reaction Conditions Optimization for Diphenylmethane:

However, although these reaction conditions were optimized for C-H activation, the example reaction used for optimization was for the conversion of fluorene to fluorenone (**Scheme 9**). The reaction used for the remainder of the project was the oxidation of diphenylmethane to

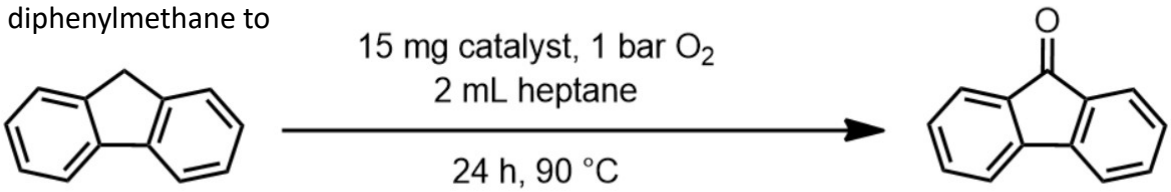

benzophenone. The C-H activation required for the oxidation of fluorene and diphenylmethane is of different difficulty for the two substances. This is because the homolytic dissociation energy of the corresponding C-H bond is higher for diphenylmethane.[45] Therefore, it is obvious that the oxidation reaction of diphenylmethane cannot achieve the conversion achieved in fluorene with the optimized conditions.

Compound	Homolytic Bond Dissociation

	Energy (BDE) kcal/mol
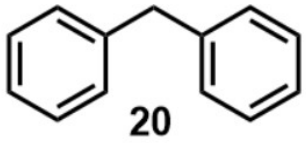 20	82
	85

Table 4: Homolytic bond dissociation Energies of fluorene and diphenylmethane

Nevertheless, optimized reaction conditions for C-H activation were tested on diphenylmethane. As expected, the conversion was 9%. Four different experiments were therefore designed to find the optimum conditions for diphenylmethane. All experiments were carried out by increasing the temperature to 120 °C. As the temperature was above the boiling point of heptane, chlorobenzene was used as the solvent.

In the first experiment the amount of catalyst was increased to 50 mg and in the second to 75 mg. In the third experiment the solvent was reduced to 1 ml to provide a more concentrated medium and the catalyst was increased to 30 mg. In the last experiment the catalyst was kept at 15 mg but the amount of diphenylmethane and solvent was halved. The aim was to increase the amount of oxygen in the Schlenk tube. When the conversion was analyzed by NMR after the experiments, it was found that the third experiment with 75 mg of catalyst gave the highest conversion and 75% yield was obtained by isolation with column chromatography. It was therefore decided to continue with the substrate range under these conditions.

(d) Mechanistic Studies for Diphenylmethane

The next step was to synthesize diarylmethanes containing electron-withdrawing and electron-donating groups and to determine the trend by performing experiments under

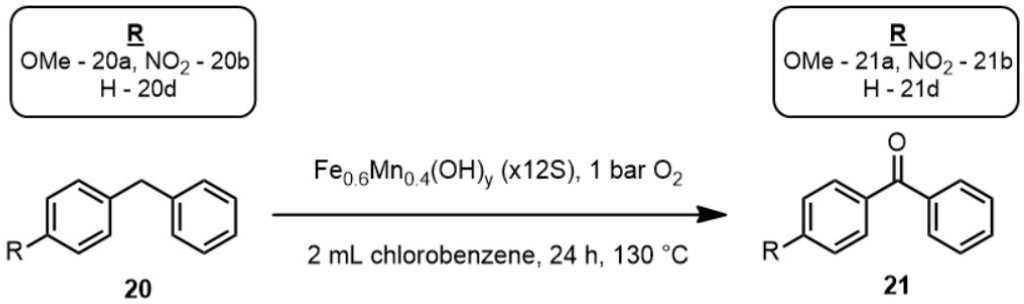

*Figure 17: (a) Oxidation reaction scheme of compounds **20a,20b** and **20c to 21a, 21b** and **21c.***

*Table 5: Isolated yields of **21a,21b** and **21c**.*

		Isolated Yields %
21a	-OMe	59
21b	-NO_2	93
21c	-H	87

This showed that the mechanism should be different. Considering that electron-withdrawing groups in carbanions increase stability, the following mechanism (**Scheme 9**) can be proposed. Molecular oxygen coordinates to the catalyst surface and forms a superoxide ion. Subsequently, the superoxide ion, acting as a base, detaches one of the benzylic protons of diphenylmethane, leading to the formation of a carbanion. The carbanion is then converted by molecular oxygen into the benzophenone. There are two lines of evidence for this mechanism. Firstly, due to isotope effect experiments, the isotope effect was calculated to be 2.2 (**Figure 18**). This proved that the proton splitting step is the rate-determining step.[46] Secondly, the fact that NO_2 functionalized diphenylmethane gives the highest yield can be explained by stabilizing the carbanion with electron-withdrawing groups.

Figure 18: Kinetic isotope effect ^{1}H-NMR spectrum.

The kinetic isotope effect was found to be 2.2 and the relatively low value of the kinetic isotope effect proves the existence of a pKa-dependent mechanism, i.e. deprotonation.[35]

A cryogenic O_2 adsorption experiment on Fe and Mn metals should first be carried out to prove the accuracy of this mechanism. In this way, it can be understood whether O_2 forms superoxide ions while coordinating to the metal as proposed.[47] In addition, it can be understood whether radicals are formed in the mechanism by experimenting with TEMPO, which is a radical trap.

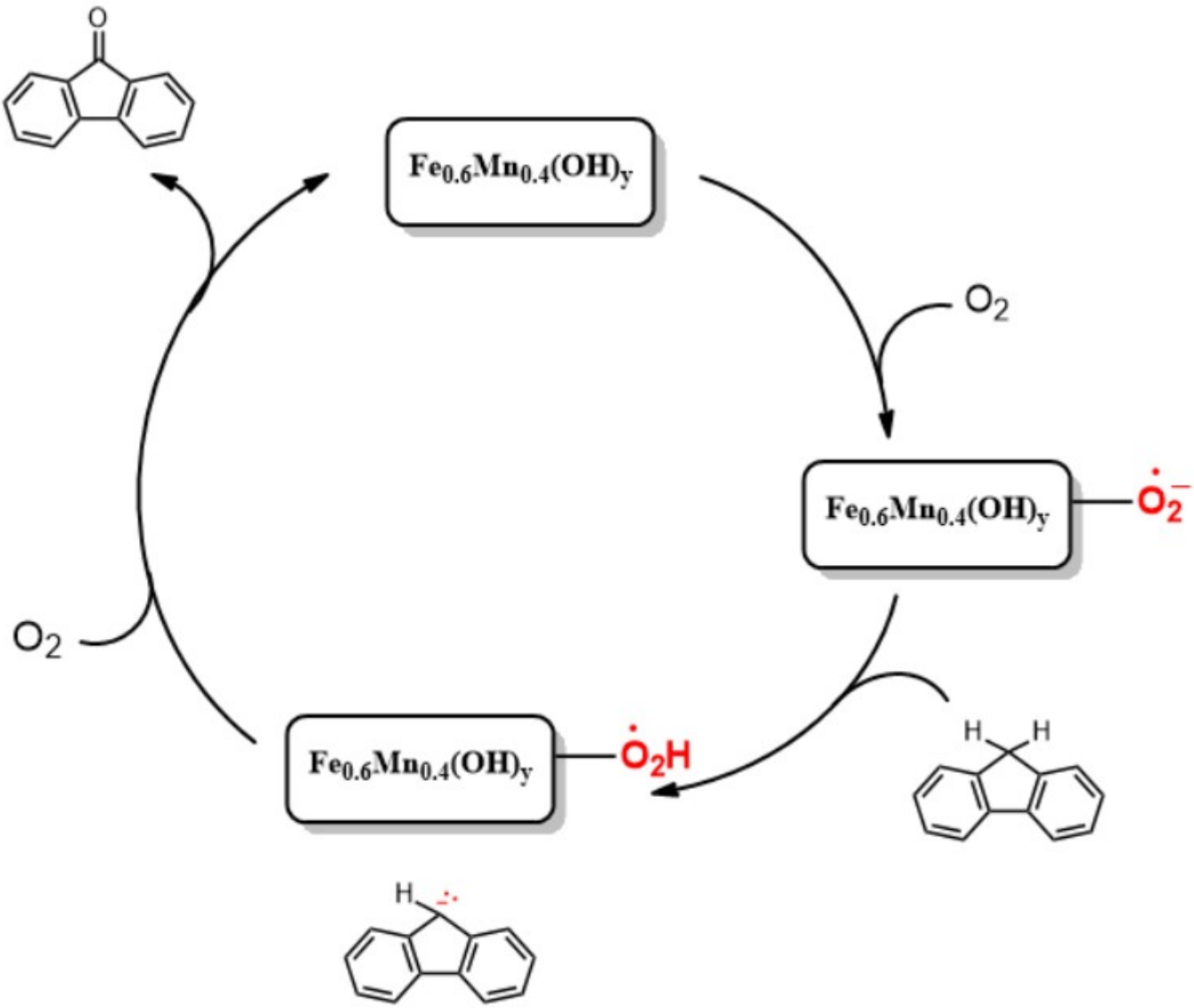
O
$Fe_{0.6}Mn_{0.4}(OH)_y$
O_2
$Fe_{0.6}Mn_{0.4}(OH)_y$
$\dot{O}_2^-$
H H
$Fe_{0.6}Mn_{0.4}(OH)_y$
$\dot{O}_2H$
O_2
H

CONCLUSION

In summary, to develop an aerobic C-H oxidation, $Fe_xMn_{1-x}(OH)_y$ catalyst was synthesized using earth abundant, environmentally friendly and inexpensive metals. The elemental ratio of Fe and Mn was optimized to $Fe_{0.6}Mn_{0.4}(OH)_y$ using fluorene to fluorenone control reaction. The best conversion was observed when the NaOH concentration used during the synthesis was 24.7 M. After the experimental conditions were optimized as 2 mL heptane, 1 bar O_2, 15 mg catalyst and 90 °C, the more difficult to oxidize diphenylmethane substrate was used. Since the reaction conditions optimized for fluorene were not sufficient, the temperature and amount of catalyst were increased.

For two diphenylmethane derivatives functionalized with OMe and NO_2 at position 4, the reaction was repeated under optimized conditions. It was observed that the diphenylmethane with NO_2 gave 93% conversion while the OMe functionalized one gave 59%. Since electron-withdrawing groups are known to stabilize anions better, the mechanism was proposed to be via the diphenylmethane anion. Kinetic isotope effect calculations revealed that the rate determining step of the mechanism was C-H bond cleavage. The kinetic isotope effect was 2.2 and such a low value supported the assumption of a pKa-dependent mechanism.

CHAPTER 3

EXPERIMENTAL SECTION

Instrumental Details

All reactions were performed using oven-dried glassware under an inert atmosphere of nitrogen. Reactions were monitored by thin-layer chromatography (TLC) using aluminum-backed plates pre-coated with silica gel (Silicycle, Silica Gel 60 F_{254}). UV light and $KMnO_4$ staining solutions were used for TLC visualization. Flash column chromatography was performed on Silicycle 40-63 λm (230-400 mesh) flash silica gel. NMR spectra were measured using a Bruker spectrometer at 400 MHz for ^{1}H-NMR spectra and 100 MHz for ^{13}C-NMR spectra and calibrated from internal standard (TMS, 0 ppm) or residual solvent signals (chloroform at 7.26 ppm for ^{1}H spectra, and at 77.16 ppm and for ^{13}C spectra). ^{1}H-NMR data are reported as follows: chemical shift (parts per million, ppm), integration, multiplicity (s = singlet, d = doublet, t = triplet, dd = doublet of doublets, m = multiplet, app = apparent), coupling constant (Hz). Infrared (FTIR) spectra were recorded on a Bruker Alpha-Platinum-ATR spectrometer with only selected peaks reported. Mass spectral analyses were performed at UNAM-National Nanotechnology Research Center and Institute of Materials Science and Nanotechnology, Bilkent University.

Experimental Details for Chapter 1

Iodonaphthalene derivatives **6a**, **6b** and **iii** were prepared following our previously reported procedures.[22]

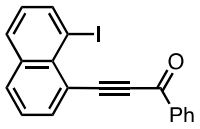

6a

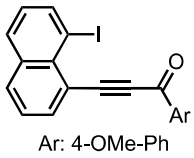

6b

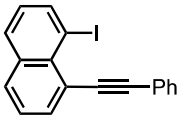

iii

(a) Synthesis of Naphthalenes 10a-10b:

10a

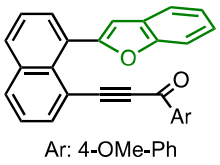

An oven-dried, round bottom flask was evacuated with vacuum and refilled with nitrogen three times. Iodonaphthalene **6b** (140 mg, 0.34 mmol) was dissolved in 1.5 mL of anhydrous 1,4-dioxane. Then, benzofuran-2-boronic acid (110 mg, 0.68 mmol) and $Pd(PPh_3)_4$ (19.6 mg, 0.017 mmol) were added sequentially. The walls of the flask were washed with additional 1,4-dioxane (1.5 mL). Finally, K_3PO_4 (217 mg, 1.02 mmol) and 1.5 mL of distilled water were added. The resulting reaction mixture was stirred in an oil bath at 100 °C with a condenser for 4.5 h. After full consumption of iodonaphthalene **6b** was observed by TLC, the reaction mixture was cooled down to ambient temperature and quenched with distilled water. Then,

the aqueous phase was extracted three times with EtOAc. The combined organic layers were dried over Na_2SO_4, filtered and concentrated under reduced pressure. Purification by flash column chromatography (EtOAc:hexanes = 1:9) gave product **10a** as red oil (88 mg, 64% yield).

R_f = 0.25 (EtOAc:hexanes = 1:6)

TLC Visualization: UV active; stains rapidly with $KMnO_4$ solution.

^{1}H NMR (400 MHz; $CDCl_3$) δ: 8.02 (2H, d, *J* = 8.2 Hz), 7.93 (1H, d, *J* = 7.2 Hz), 7.75 (1H, d, *J* = 6.9 Hz), 7.66 (2H, d, *J* = 8.5 Hz), 7.61 (1H, t, *J* = 7.6 Hz), 7.55 (1H, t, *J* = 7.8 Hz), 7.22 (2H, t, *J* = 7.9 Hz), 7.01 (1H, t, *J* = 7.4 Hz), 6.95 (1H, t, *J* = 7.5 Hz), 6.87 (1H, s), 6.80 (2H, d, *J* = 8.7 Hz), 3.88 (3H, s).

^{13}C NMR (100 MHz; $CDCl_3$) δ: 175.5, 164.0, 155.8, 154.2, 135.5, 134.2, 132.4, 131.7, 131.6, 131.1, 131.0, 129.8, 129.3, 128.6, 125.9, 125.6, 124.3, 122.8, 121.0, 117.8, 113.2, 111.8, 106.9, 91.5, 91.1, 55.6.

FTIR ν_{max} (ATR, film)/cm^{-1} 3054, 2921, 2851, 2188, 1738, 1664, 1598, 1573, 1508, 1457, 1421, 1371, 1256, 1236, 1162, 1108, 1028, 953, 882, 829, 750.

HRMS (+ESI) Calcd for $C_{28}H_{19}O_2$ $[M+H]^+$ 403.1329, found: 403.1324.

10b

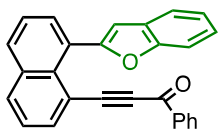

An oven-dried, round bottom flask was evacuated with vacuum and refilled with nitrogen three times. Iodonaphthalene **i** (133 mg, 0.348 mmol) was dissolved in 1.0 mL of anhydrous 1,4-dioxane. Then, benzofuran-2-boronic acid (134 mg, 0.83 mmol) and $Pd(PPh_3)_4$ (20 mg, 0.017 mmol) were added sequentially. The walls of the flask were washed with additional 1,4-dioxane (1.0 mL). Finally, K_3PO_4 (222 mg, 1.05 mmol) and 1.0 mL of distilled water were added. The resulting reaction mixture was stirred in an oil bath at 100 °C with a condenser for 6.5 h. After full consumption of iodonaphthalene **i** was observed by TLC, the reaction mixture was cooled down to ambient temperature and quenched with distilled water. Then, the aqueous phase was extracted three times with EtOAc. The combined organic layers were dried over Na_2SO_4, filtered and concentrated under reduced pressure. Purification by flash column chromatography (only hexanes) gave product **10b** as orange oil (91 mg, 70% yield).

R_f = 0.48 (EtOAc:hexanes = 1:4)

TLC Visualization: UV active; stains with $KMnO_4$ solution.

^{1}H NMR (400 MHz; $CDCl_3$) δ: 8.03 (2H, d, *J* = 8.2 Hz), 7.94 (1H, d, *J* = 7.0 Hz), 7.75 (1H, d, *J* = 6.7 Hz), 7.70 (2H, d, *J* = 7.3 Hz), 7.63 – 7.49 (3H, m), 7.33 (2H, t, *J* = 7.7 Hz), 7.21 (1H, d, *J* = 8.1 Hz), 7.16 (1H, d, *J* = 7.3 Hz), 6.99 (1H, td, *J* = 8.0, 1.2 Hz), 6.93 (1H, t, *J* = 7.4 Hz), 6.87 (1H, s).

^{13}C NMR (100 MHz; $CDCl_3$) δ: 176.8, 155.8, 154.2, 136.3, 135.6, 134.3, 133.6, 132.5, 131.7, 131.3, 131.1, 129.4, 129.3, 128.7, 128.0, 126.0, 125.7, 124.4, 122.9, 121.0, 117.7, 111.9, 107.0, 91.9.

FTIR ν_{max} (ATR, film)/cm^{-1} 3060, 2956, 2921, 2851, 2188, 1733, 1635, 1616, 1598, 1450, 1372, 1354, 1258, 1228, 1175, 1097, 1019, 952, 907.

HRMS (+ESI) Calcd for $C_{27}H_{17}O_2$ $[M+H]^+$ 373.1223, found: 373.1216.

(b) Synthesis of Control Substances

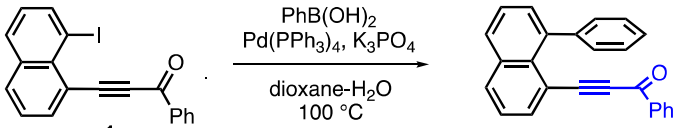

i **11**

An oven-dried, round bottom flask was evacuated with vacuum and refilled with nitrogen three times. Iodonaphthalene **i** (35 mg, 0.092 mmol) was dissolved in 1.0 mL of anhydrous 1,4-dioxane. Then, phenylboronic acid (22.9 mg, 0.188 mmol) and $Pd(PPh_3)_4$ (5.4 mg, 0.005 mmol) were added sequentially. The walls of the flask were washed with additional 1,4-dioxane (1.0 mL). Finally, K_3PO_4 (60 mg, 0.28 mmol) and 1.0 mL of distilled water were added. The resulting reaction mixture was stirred in an oil bath at 100 °C with a condenser for 3.5 h. After full consumption of iodonaphthalene **i** was observed by TLC, the reaction mixture was cooled down to ambient temperature and quenched with distilled water. Then, the aqueous phase was extracted three times with EtOAc. The combined organic layers were dried over Na_2SO_4, filtered and concentrated under reduced pressure. Purification by flash column chromatography (EtOAc:hexanes = 1:7) gave product **11** as yellow-orange solid (31 mg, 100% yield).

$\mathbf{R_f}$ = 0.47 (only hexanes)

TLC Visualization: UV active; stains slowly with $KMnO_4$ solution.

^{1}H NMR (400 MHz; $CDCl_3$) δ: 8.02 (1H, dd, *J* = 8.2, 1.1 Hz), 7.92 (1H, dd, *J* = 8.2, 1.2 Hz), 7.88 – 7.85 (3H, m), 7.59 – 7.55 (2H, m), 7.51 (1H, dd, *J* = 8.1, 7.3 Hz), 7.46 (1H, dd, *J* = 7.1, 1.3 Hz), 7.44 – 7.40 (4H, m), 7.17 (2H, app t, *J* = 7.6 Hz), 7.05 (1H, tt, *J* = 7.5, 1.2 Hz).

^{13}C NMR (100 MHz; $CDCl_3$) δ: 177.8, 141.9, 140.5, 136.9, 135.6, 134.4, 133.8, 131.6, 131.2, 130.4, 130.3, 129.8, 128.7, 128.3, 128.1, 128.0, 126.1, 125.2, 117.8, 94.6, 93.3.

FTIR ν_{max} (ATR, film)/cm^{-1} 3056, 2957, 2925, 2853, 2182, 1730, 1635, 1597, 1579, 1503, 1490, 1448, 1426, 1371, 1353, 1313, 1277.

HRMS (+ESI) Calcd for $C_{25}H_{17}O$ $[M+H]^+$ 333.1274, found: 333.1267.

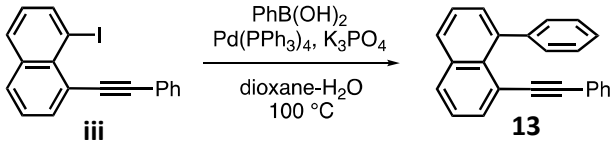

iii **13**

An oven-dried, round bottom flask was evacuated with vacuum and refilled with nitrogen three times. Iodonaphthalene **iii** (35 mg, 0.099 mmol) was dissolved in 1.0 mL of anhydrous 1,4-dioxane. Then, phenylboronic acid (24.1 mg, 0.198 mmol) and $Pd(PPh_3)_4$ (5.7 mg, 0.005 mmol) were added sequentially. The walls of the flask were washed with additional 1,4-dioxane (1.0 mL). Finally, K_3PO_4 (63 mg, 0.30 mmol) and 1.0 mL of distilled water were added. The resulting reaction mixture was stirred in an oil bath at 100 °C with a condenser for 4.5 h. After full consumption of iodonaphthalene **iii** was observed by TLC, the reaction mixture was cooled down to ambient temperature and quenched with distilled

water. Then, the aqueous phase was extracted three times with EtOAc. The combined organic layers were dried over Na_2SO_4, filtered and concentrated under reduced pressure. Purification by flash column chromatography (only hexanes) gave product **13** as white solid with a brown tinge (24 mg, 80% yield).

R_f = 0.42 (only hexanes)

TLC Visualization: Weakly UV active; stains slowly with $KMnO_4$ solution.

^{1}H NMR (400 MHz; $CDCl_3$) δ: 7.92 (1H, d, *J* = 8.2 Hz), 7.89 (1H, d, *J* = 8.2 Hz), 7.81 (1H, d, *J* = 7.2 Hz), 7.55 – 7.47 (4H, m), 7.41 – 7.36 (3H, m), 7.28 (1H, app t, *J* = 8.0 Hz), 7.22 – 7.18 (3H, m), 7.03 – 7.01 (2H, m).

^{13}C NMR (100 MHz; $CDCl_3$) δ: 143.0, 140.8, 135.0, 134.7, 131.8, 130.6, 130.5, 130.3, 129.7, 128.7, 127.8, 127.6, 127.4, 125.5, 125.3, 123.7, 120.8, 98.1, 90.3.

FTIR ν_{max} (ATR, film)/cm^{-1} 3079, 2249, 1570, 1373.

HRMS (+APCI) Calcd for $C_{24}H_{17}$ $[M+H]^+$ 305.1325, found: 305.1326.

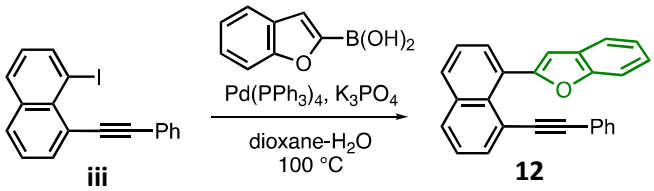

iii **12**

An oven-dried, round bottom flask was evacuated with vacuum and refilled with nitrogen three times. Iodonaphthalene **iii** (35 mg, 0.099 mmol) was dissolved in 0.5 mL of anhydrous 1,4-dioxane. Then, benzofuran-2-boronic acid (32.1 mg, 0.198 mmol) and $Pd(PPh_3)_4$ (5.7 mg, 0.005 mmol) were added sequentially. The walls of the flask were washed with additional 1,4-dioxane (1.5 mL). Finally, K_3PO_4 (63 mg, 0.30 mmol) and 1.0 mL of distilled

water were added. The resulting reaction mixture was stirred in an oil bath at 100 °C with a condenser for 5 h. After full consumption of iodonaphthalene **iii** was observed by TLC, the reaction mixture was cooled down to ambient temperature and quenched with distilled water. Then, the aqueous phase was extracted three times with EtOAc. The combined organic layers were dried over Na_2SO_4, filtered and concentrated under reduced pressure. Purification by flash column chromatography (only hexanes) gave **12** as a slightly impure solid. Further recrystallization from heptane gave pure product **12** as yellow solid (25 mg, 74% yield).

R_f = 0.25 (only hexanes)

TLC Visualization: UV active; stains with $KMnO_4$ solution.

^{1}H NMR (400 MHz; $CDCl_3$) δ: 7.99 (1H, d, *J* = 8.1 Hz), 7.92 (1H, d, *J* = 8.2 Hz), 7.88 (1H, d, *J* = 7.1 Hz), 7.69 (1H, d, *J* = 6.9 Hz), 7.60 – 7.46 (4H, m), 7.23 – 7.18 (2H, m), 7.07 (1H, t, *J* = 7.2 Hz), 6.99 – 6.94 (3H, m), 6.47 (2H, d, *J* = 7.2 Hz).

^{13}C NMR (100 MHz; $CDCl_3$) δ: 157.3, 155.3, 135.3, 134.5, 131.7, 131.6, 131.2, 131.1, 129.9, 129.5, 128.9, 127.7, 127.5, 125.8, 125.4, 124.2, 123.1, 122.8, 121.0, 120.7, 111.9, 105.7, 95.2, 88.5.

FTIR ν_{max} (ATR, film)/cm^{-1} 3053, 2963, 2923, 2850, 1733, 1668, 1597, 1566, 1489, 1474, 1450, 1426, 1371, 1304, 1255, 1178, 1053, 962, 882.

HRMS (+ESI) Calcd for $C_{26}H_{17}O$ $[M+H]^+$ 345.1274, found: 345.1264

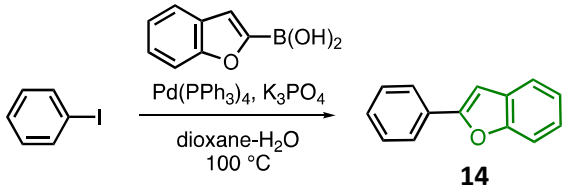

14

Anhydrous 1,4-dioxane was deoxygenated by purging nitrogen gas for 15 min. An oven-dried, round bottom flask was evacuated with vacuum and refilled with nitrogen three times. Iodobenzene (183 mg, 100 μL, 0.90 mmol) was dissolved in 1.0 mL of anhydrous 1,4-dioxane. Then, benzofuran-2-boronic acid (159 mg, 0.98 mmol) and $Pd(PPh_3)_4$ (56.6 mg, 0.049 mmol) were added sequentially. The walls of the flask were washed with additional 1,4-dioxane (4.0 mL). Finally, K_3PO_4 (624 mg, 2.94 mmol) and 2.5 mL of distilled water were added. The resulting reaction mixture was stirred in an oil bath at 100 °C with a condenser for 4.5 h. The reaction mixture was then cooled down to ambient temperature and quenched with distilled water. Then, the aqueous phase was extracted three times with EtOAc. The combined organic layers were dried over Na_2SO_4, filtered and concentrated under reduced pressure. Purification by flash column chromatography (only hexanes) gave product **14** as white solid (70 mg, 40% yield).

R_f = 0.69 (only hexanes)

TLC Visualization: UV active; stains slowly with $KMnO_4$ solution.

^{1}H NMR (400 MHz; $CDCl_3$) δ: 7.93 (2H, d, *J* = 7.4 Hz), 7.64 (1H, d, *J* = 7.4 Hz), 7.60 (1H, d, *J* = 7.9 Hz), 7.50 (2H, t, *J* = 7.5 Hz), 7.41(1H, t, *J* = 7.3 Hz), 7.34 (1H, t, *J* = 7.5 Hz), 7.30 (1H, t, *J* = 7.3 Hz), 7.07 (1H, s).

^{13}C NMR (100 MHz; $CDCl_3$) δ: 156.0, 155.0, 130.6, 129.4, 128.9, 128.7, 125.1, 124.4, 123.1, 121.0, 111.3, 101.4.

FTIR ν_{max} (ATR, film)/cm^{-1} 3053, 2926, 2854, 2200, 1642, 1491, 1455, 1443, 1264.

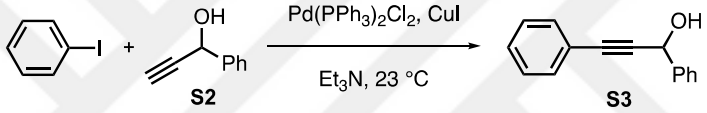

An oven-dried 25-mL Schlenk tube was evacuated with vacuum and refilled with nitrogen three times. Iodobenzene (100 mg, 55 μL, 0.49 mmol) and alkyne **S2** (65 mg, 0.50 mmol) were dissolved in 1.5 mL of Et_3N. Then, $Pd(PPh_3)_2Cl_2$ (24.5 mg, 0.035 mmol) and CuI (13.3 mg, 0.070 mmol) were added sequentially. The walls of the flask were washed with additional Et_3N (2.5 mL). The reaction mixture was stirred at 23 °C for 4 h. After the completion of the reaction, Et_3N was removed under reduced pressure. Distilled water was added to the mixture, and the aqueous phase was extracted three times with CH_2Cl_2. The combined organic layers were dried over Na_2SO_4, filtered and concentrated under reduced pressure. Purification by flash column chromatography (EtOAc:hexanes = 1:4) gave pure product **S3** (47 mg, 46% yield). The ^{1}H-NMR spectroscopic data match those reported in the literature.[48]

^{1}H NMR (400 MHz; $CDCl_3$) δ: 7.64 (2H, d, *J* = 7.2 Hz), 7.50 – 7.48 (2H, m), 7.42 (2H, t, *J* = 7.2 Hz), 7.38 – 7.31 (4H, m), 5.70 (1H, s), 2.48 (1H, s).

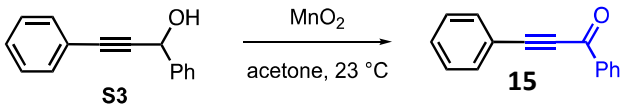

S3 **15**

To a solution of the propargylic alcohol **S3** (47 mg, 0.23 mmol) in 10 mL of acetone in a 20-mL vial was added MnO_2 (393 mg, 4.52 mmol) at 23 °C. The reaction mixture was stirred for 3 h and then filtered to remove all solids. All volatiles were then removed under reduced pressure. Purification by flash column chromatography (EtOAc:hexanes = 1:7) gave pure ynone product **15** (17 mg, 36% yield). The ^{1}H-NMR spectroscopic data match those reported in the literature.[49]

^{1}H NMR (400 MHz; $CDCl_3$) δ: 8.23 (2H, d, *J* = 7.7 Hz), 7.69 (2H, d, *J* = 7.0 Hz), 7.64 (1H, t, *J* = 7.3 Hz), 7.54 – 7.47 (3H, m), 7.43 (2H, t, *J* = 7.6 Hz).

^{1}H- and ^{13}C{^{1}H}-NMR Spectra Related to Chapter 1:

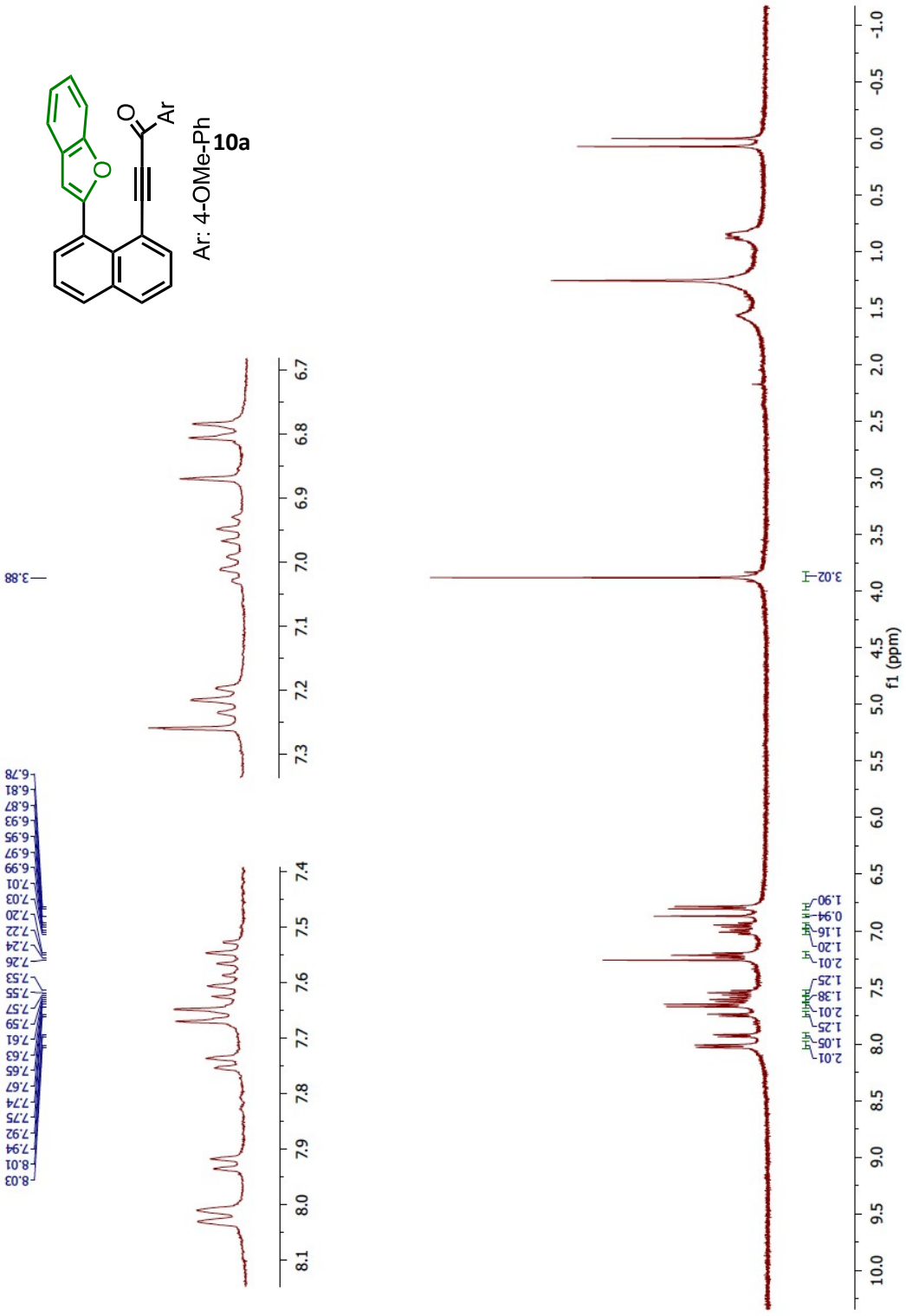

*Proton NMR 1:. ^{1}H-NMR spectrum of **10a** in $CDCl_3$.*

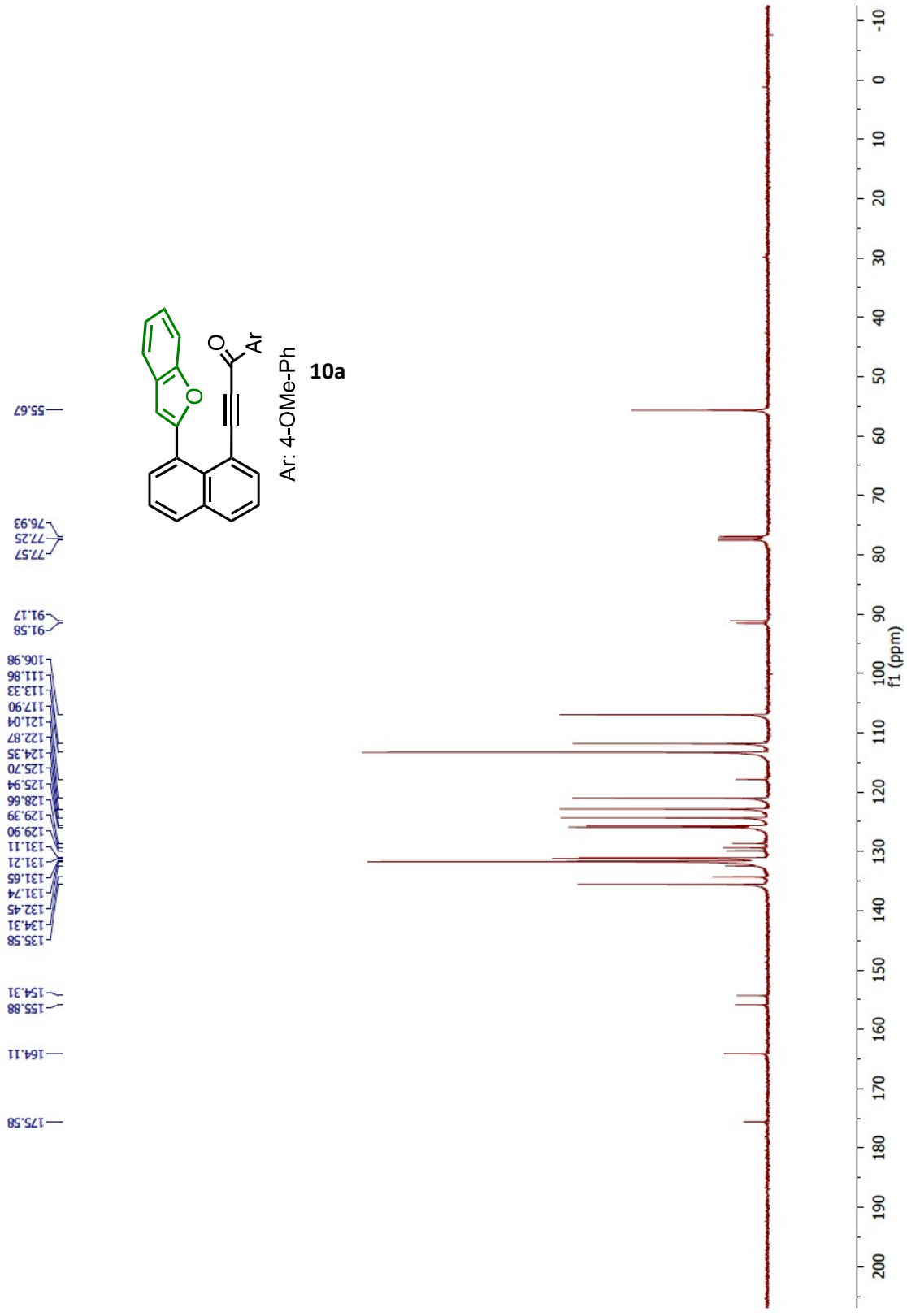

*Carbon NMR 1: $^{13}C\{^{1}H\}$-NMR spectrum of **10a** in $CDCl_3$.*

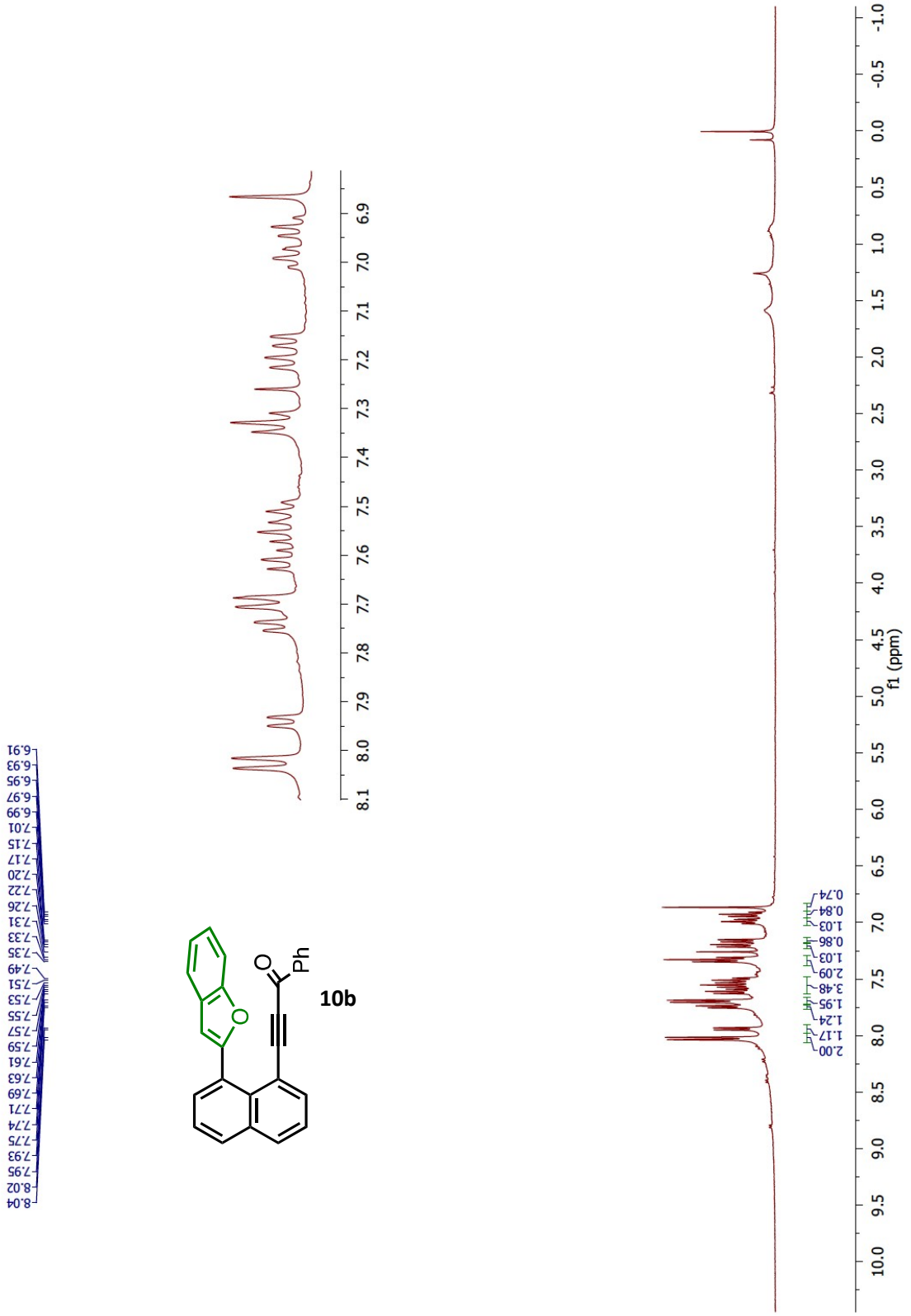

*Proton NMR 2: ^{1}H-NMR spectrum of **10b** in $CDCl_3$.*

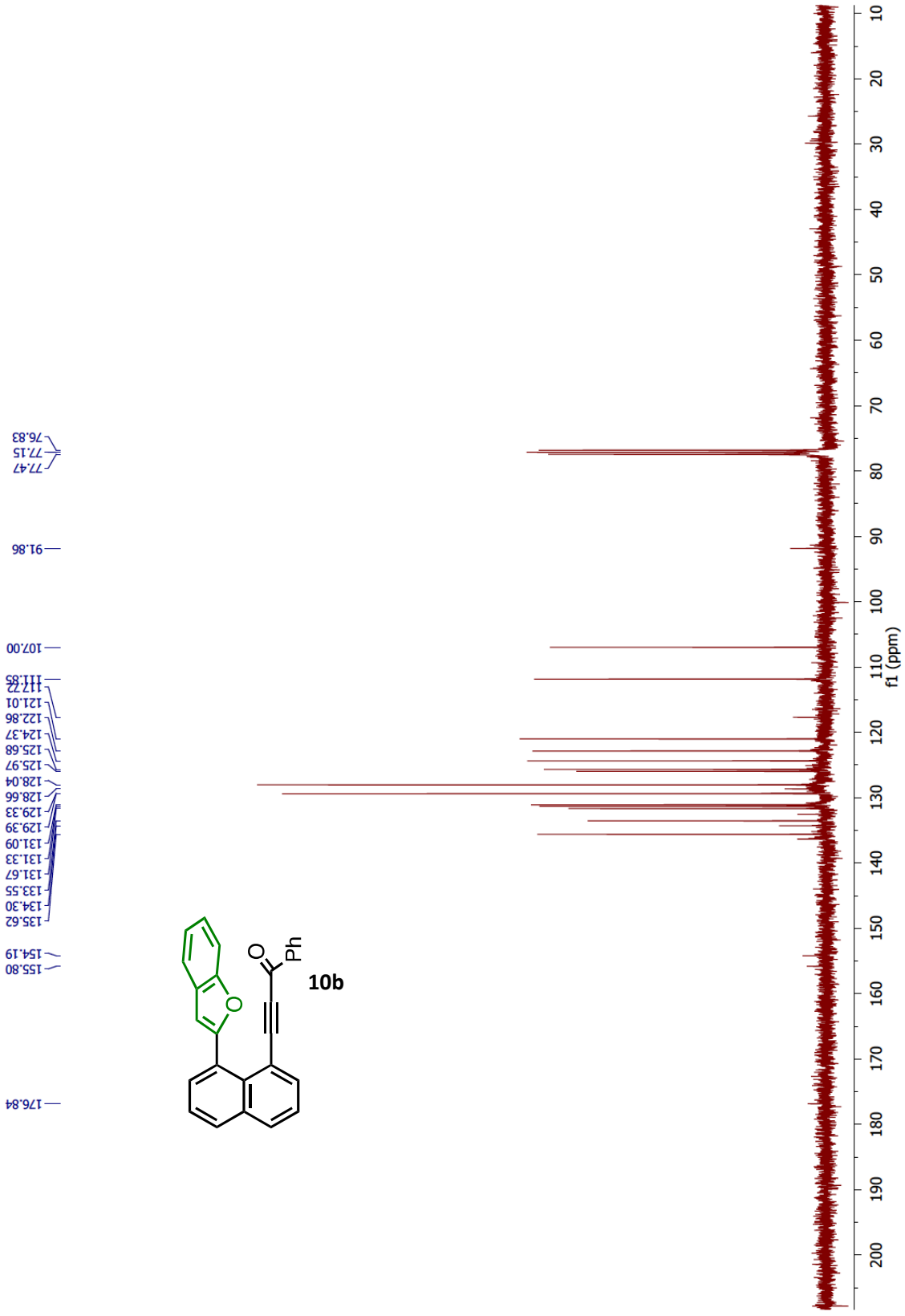

*Carbon NMR 2: $^{13}C\{^{1}H\}$-NMR spectrum of **10b** in $CDCl_3$.*

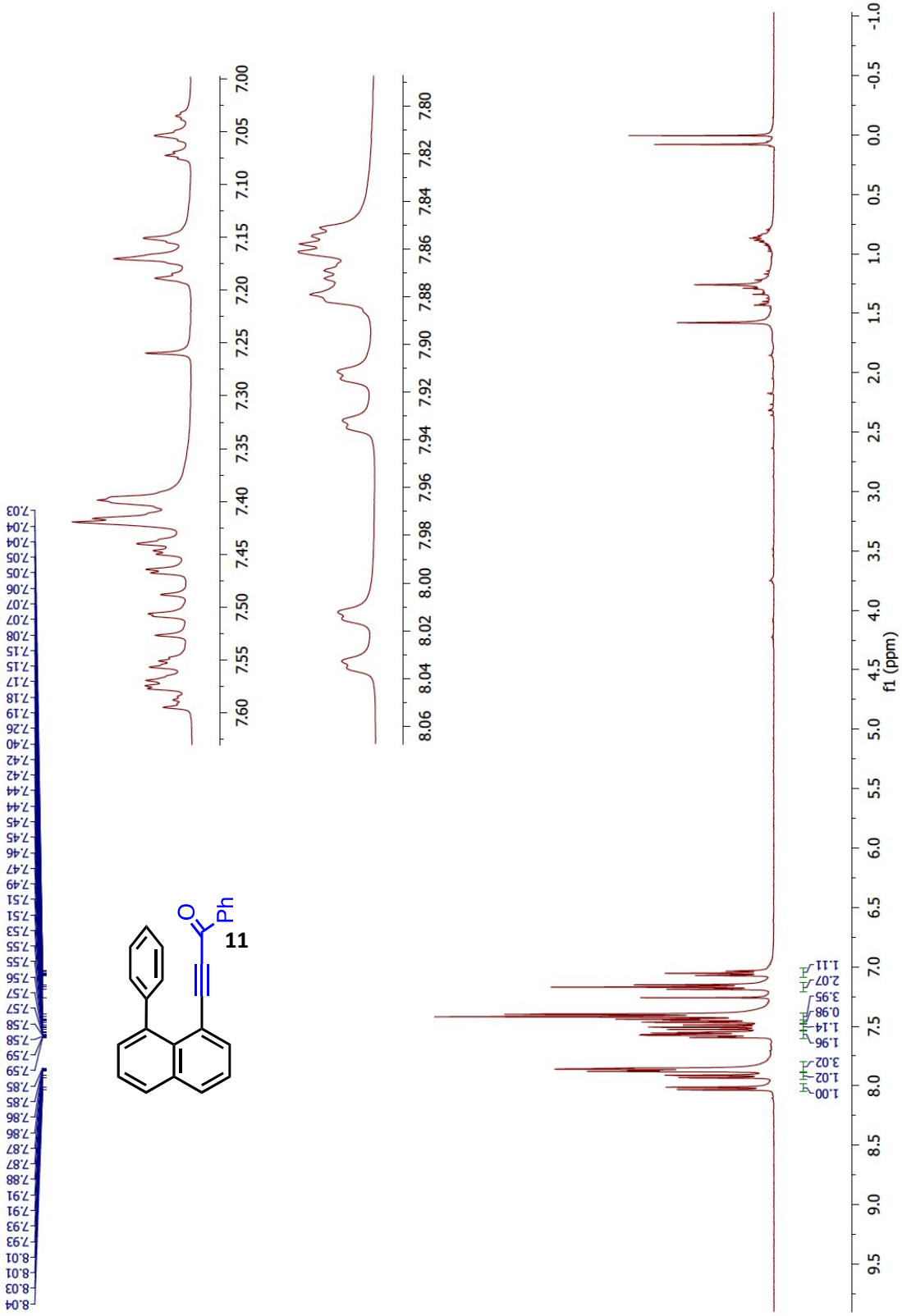

*Proton NMR 3: ^{1}H-NMR spectrum of **11** in $CDCl_3$.*

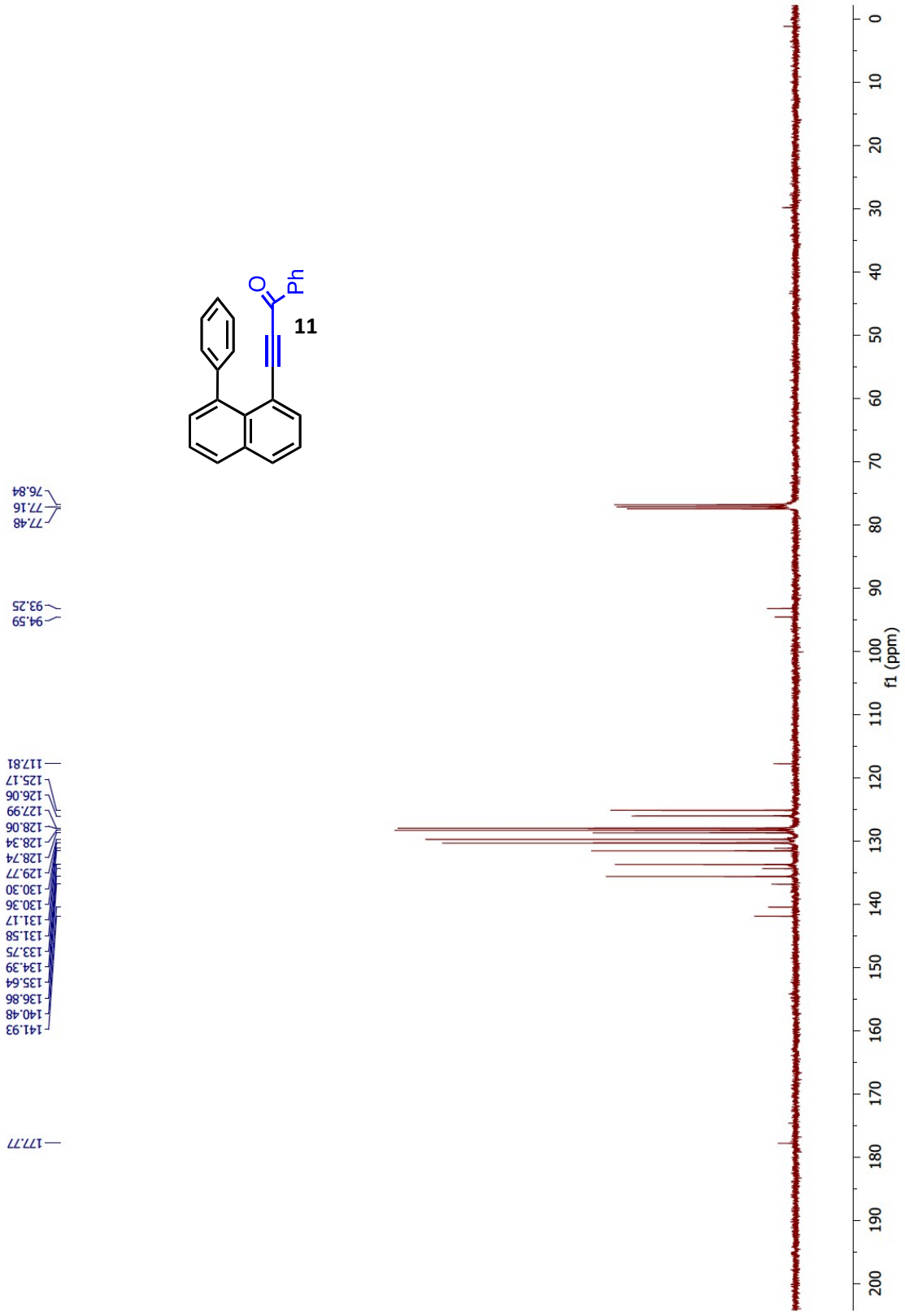

*Carbon NMR 3: $^{13}C\{^{1}H\}$-NMR spectrum of **11** in $CDCl_3$.*

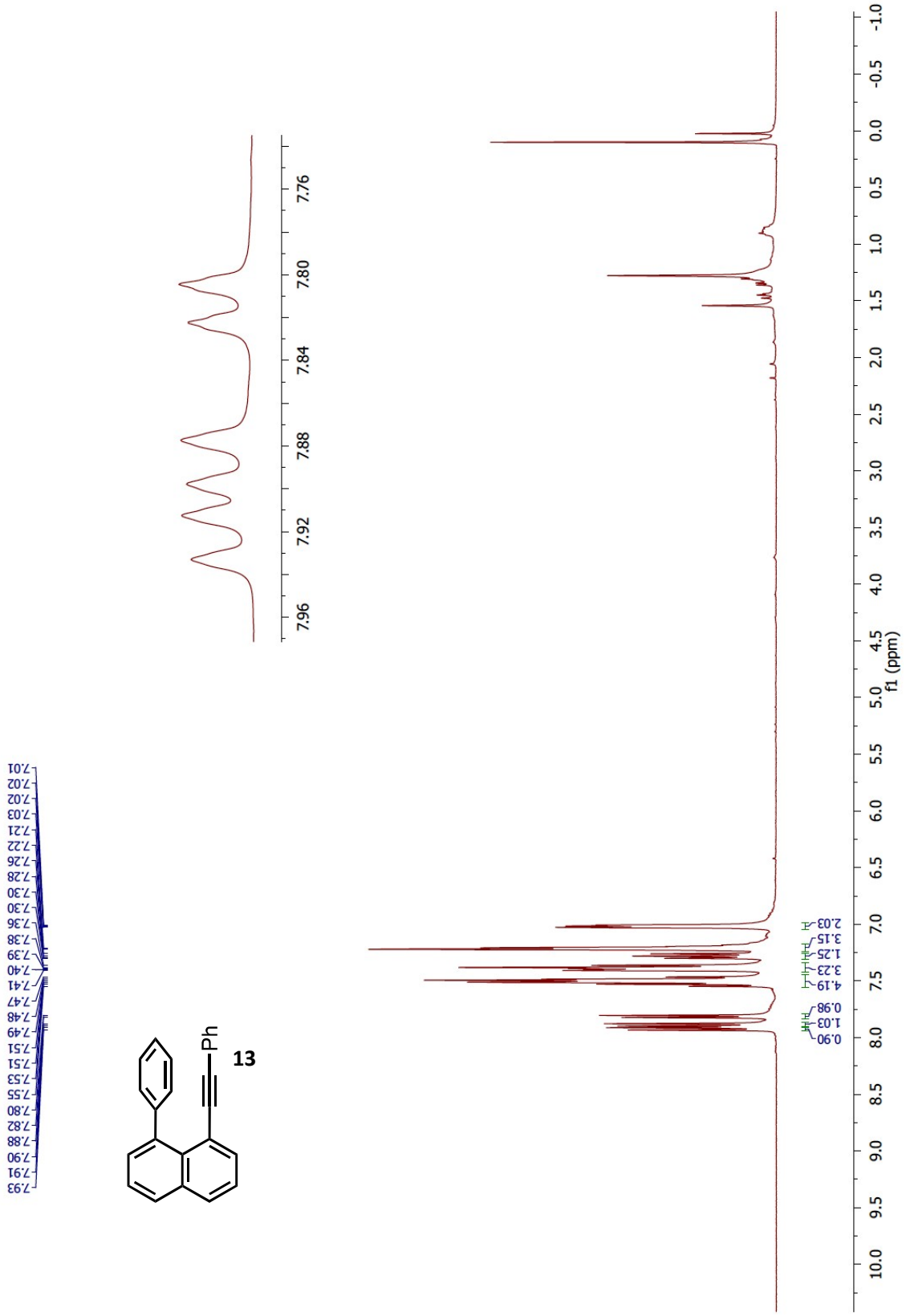

*Proton NMR 4: ^{1}H-NMR spectrum of **13** in $CDCl_3$.*

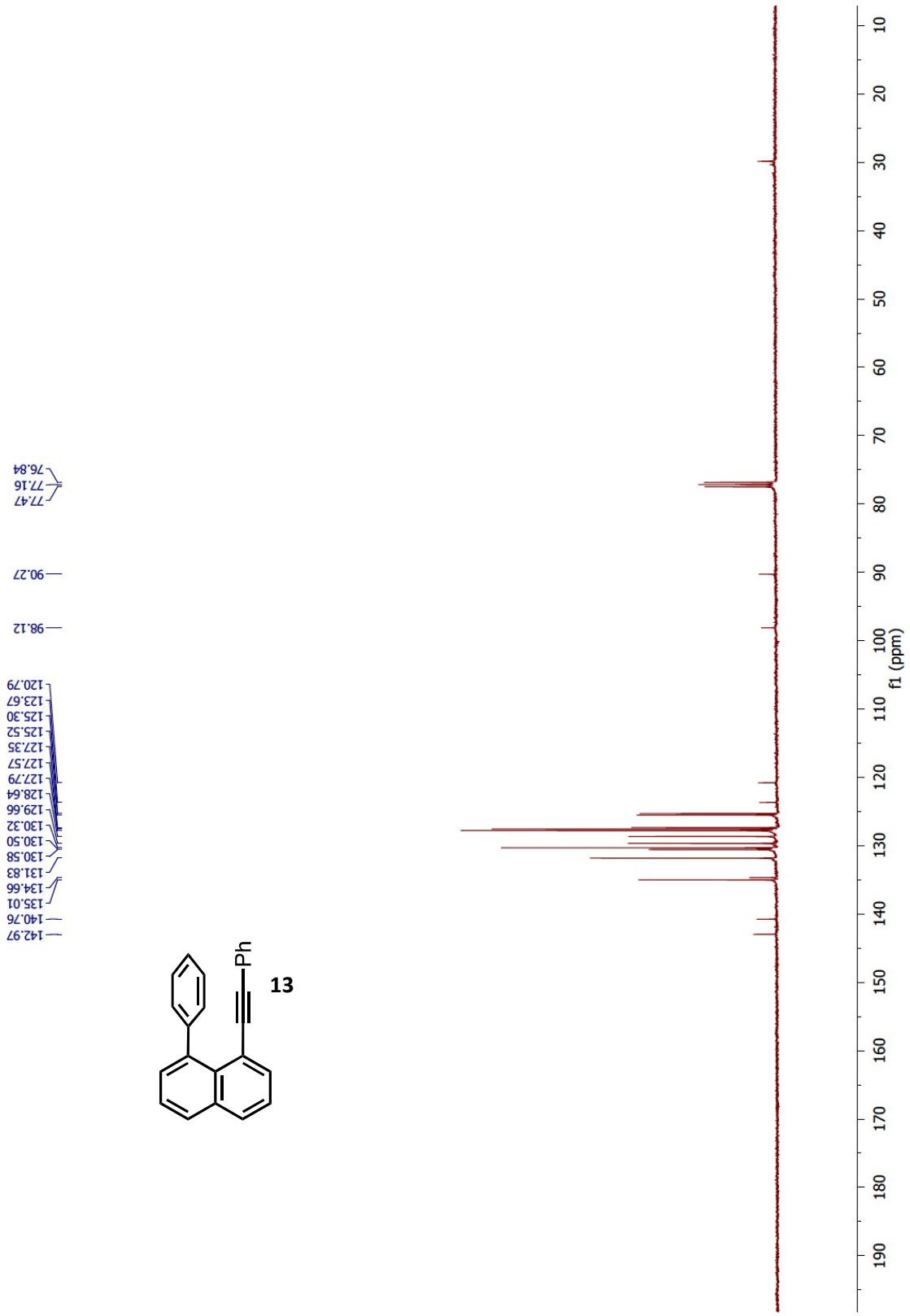

*Carbon NMR 4: $^{13}C\{^{1}H\}$-NMR spectrum of **13** in $CDCl_3$.*

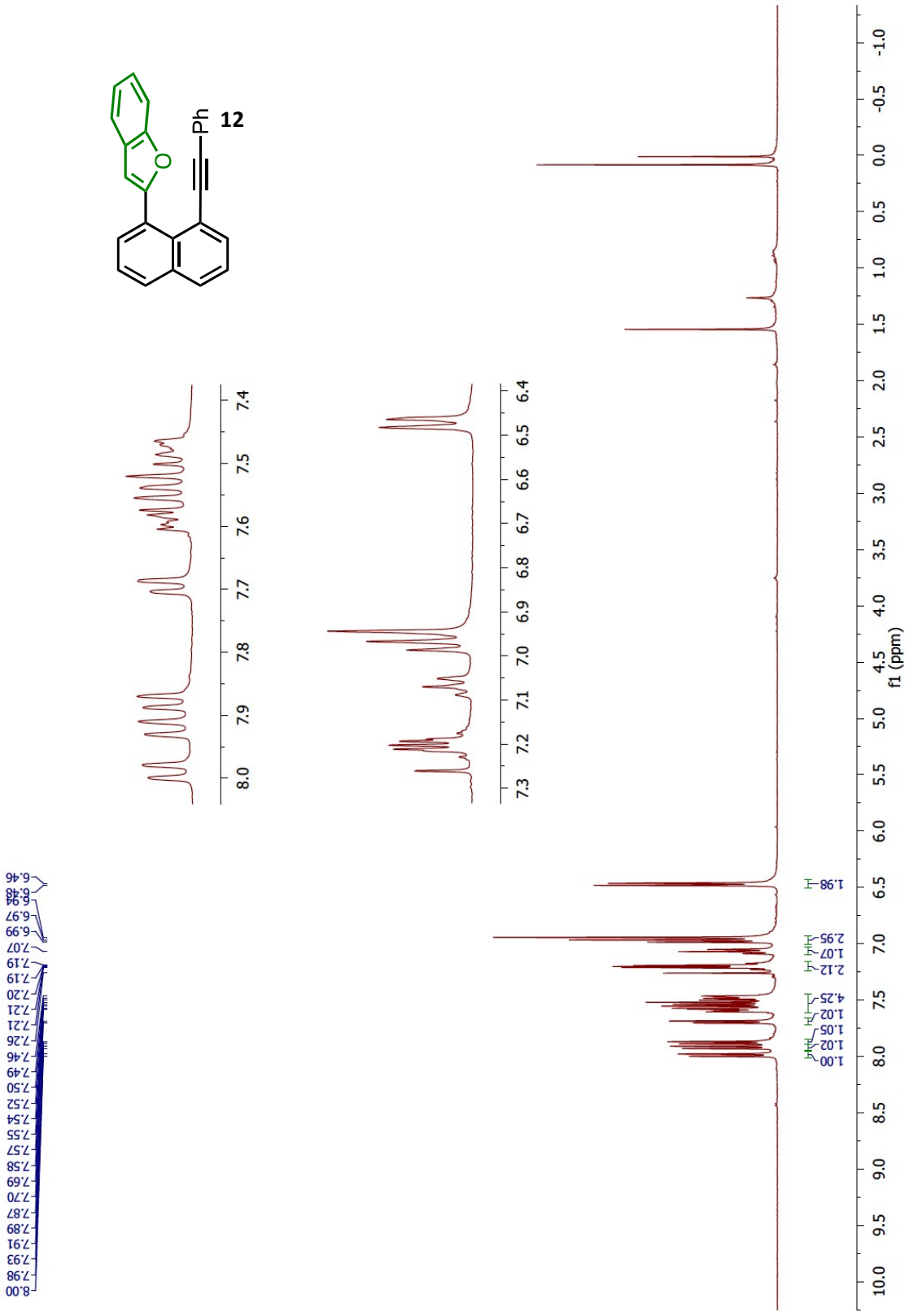

*Proton NMR 5: ^{1}H-NMR spectrum of **12** in $CDCl_3$.*

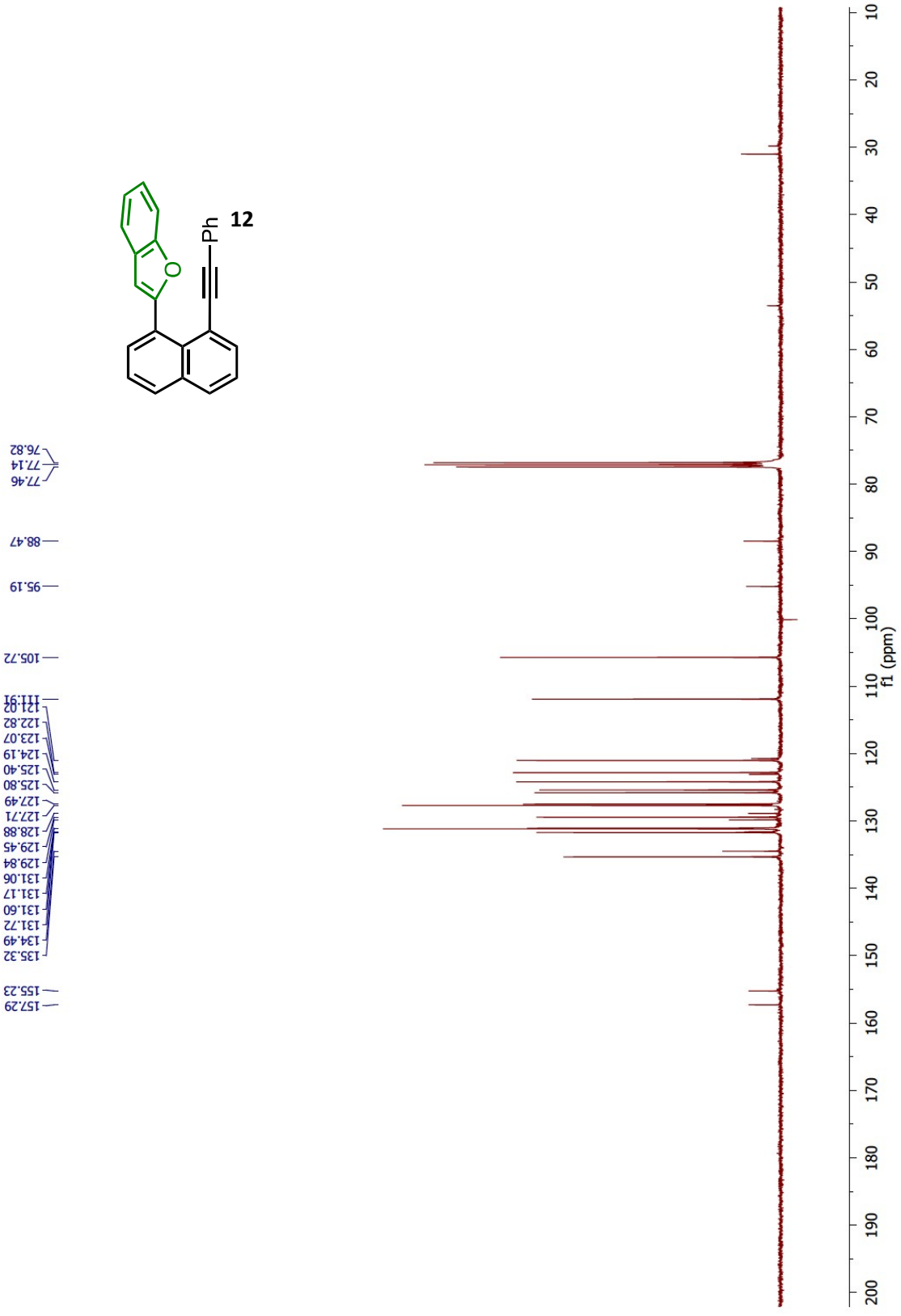

*Carbon NMR 5: $^{13}C\{^{1}H\}$-NMR spectrum of **12** in $CDCl_3$.*

Experimental Details of Chapter 2

(c) Recrystallization of Fluorene (18):

2.0 g of fluorene in a beaker was placed on a 70 °C heater to dissolve in 50 ml of ethanol. After complete dissolution, the beaker was cooled to room temperature. The beaker was covered with aluminum foil and holes were punched in the foil. After some ethanol had evaporated, the crystals were filtered with a suction filter. The crystals were allowed to dry on the filter paper, then transferred to a beaker and placed under vacuum until the solvent was completely removed. The colour of the purchased fluorene was off-white, whereas the colour of the recrystallized fluorene was bright white.

(d) General Optimized Procedure for Fluorene (18) to Fluorenone (19) Reaction:

In oven dried Schlenk tube, 0.5mmol (83.12mg) recrystallized fluorene was placed after the flask was cooled down to room temperature, Then, 10mg $Fe_{0.6}Mn_{0.4}$ (OH) (x12S) catalyst was added and 2ml heptane was added by washing the walls of the flask. Then grease was applied to the connection part of the flask and the tap. After that, plastic clamp was placed, and the connection part was wrapped by parafilm 3 times. Inside of the flask was washed with oxygen gas and the tap which is placed on the top was closed. Then 1 bar of oxygen was applied for 30 seconds, and the other tap was closed. Finally, the Schlenk tube was placed in oil bath at 80°C and 400rpm. After 24 hours, the catalyst was removed by using celite and EtOAc. Then, EtOAc was evaporated and by using $CDCl_3$, ^{1}H-NMR data was obtained. The conversion was calculated according to the ^{1}H-NMR data.

(e) General procedure for Diphenylmethane (20) synthesis[50]

An oven-dried 25 mL Schlenk tube was evacuated with vacuum and refilled three times with nitrogen. Pd(PPh3)3Cl2 and Na2CO3 were added and dissolved in 1 mL THF and 1 mL water. Benzyl chloride and phenylboronic acid derivative were then added sequentially. Finally, the walls of the tube were washed with 0.5 mL THF and 0.5 mL water. The resulting reaction mixture was stirred in an oil bath at 40 °C for 24 h. The aqueous phase was then extracted three times with EtOAc. The combined organic layers were dried over Na2SO4, filtered and concentrated under reduced pressure. Purification by flash column chromatography (hexanes only) afforded product 5a as orange oil (91 mg, 70% yield).

(f) General Optimized Procedure for Oxidation of diphenylmethane derivatives:

In oven dried Schlenk tube, 0.25mmol diphenylmethane derivative was placed after the flask was cooled down to room temperature, Then, 37 mg $Fe_{0.6}Mn_{0.4}$ (OH) (x12S) catalyst was added and 2ml chlorobenzene was added by washing the walls of the flask. Then grease was applied to the connection part of the flask and the tap. After that, plastic clamp was placed, and the connection part was wrapped by parafilm 3 times. Inside of the flask was washed with oxygen gas and the tap which is placed on the top was closed. Then 1 bar of oxygen was applied for 30 seconds and the other tap was closed. Finally, the Schlenk tube was placed in oil bath at 130°C and 400rpm. After 24 hours, chlorobenzene The mixture was treated with reduced pressure to remove it, followed by the addition of EtOAc., the catalyst was removed by filtering through celite. Then, EtOAc was evaporated and by using $CDCl_3$, ^{1}H-NMR data was obtained. The conversion was calculated according to the ^{1}H-NMR data.

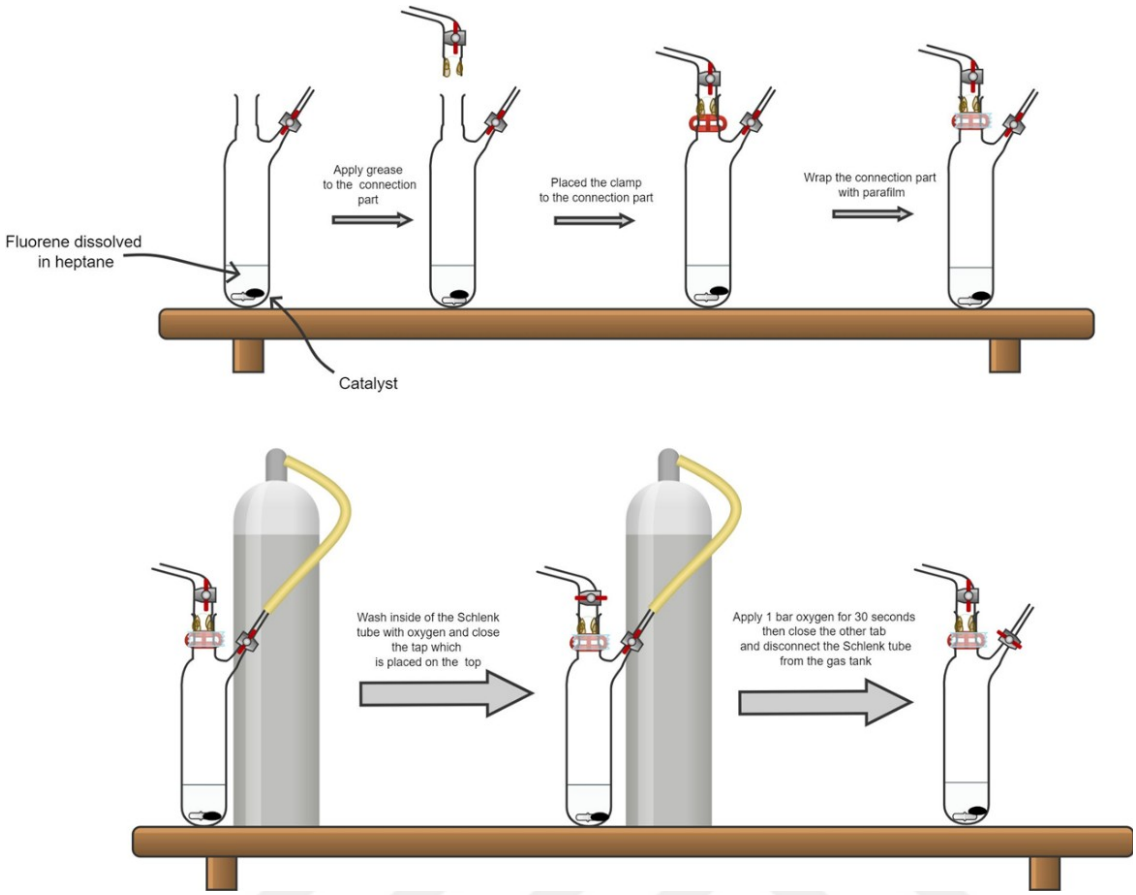

(g) Kinetic İsotope Effect Calculations

$$Fluorene + Deutoreted\ Fluorene \rightarrow Fluoerone \qquad 0.25\,mmol\ 0.25\,mmol \rightarrow -¿$$

$$\frac{-x\,mmol - y\,mmol \rightarrow x + y\,mmol}{0.25 - x\,mmol\ 0.25 - y\,mmol \rightarrow x + y\,mmol}$$

$$0.25\,mmol - x\,mmol = n \qquad 0.25\,mmol - y\,mmol = 1.075\,n \qquad x\,mmol + y\,mmol = 0.245\,n$$

$$n = 0.22 \quad x = 0.03 \quad y = 0.0135 \qquad \frac{x}{y} = 2.22 \rightarrow Kinetic\ isotope\ effect$$

1H- and 13C{1H}-NMR Spectra Related to Chapter 2:

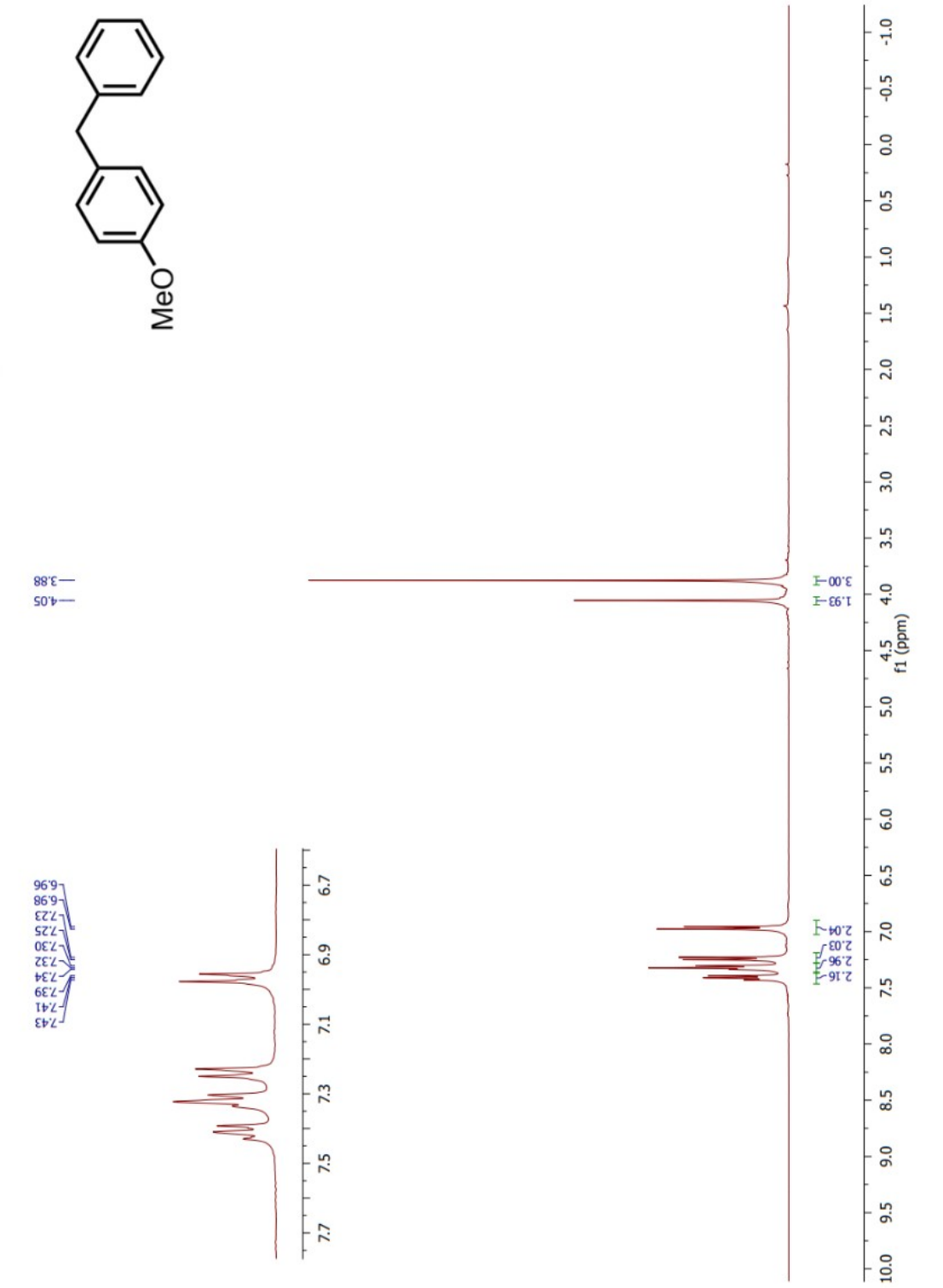

*Proton NMR 6: ^{1}H-NMR spectrum of **20a** in $CDCl_3$*

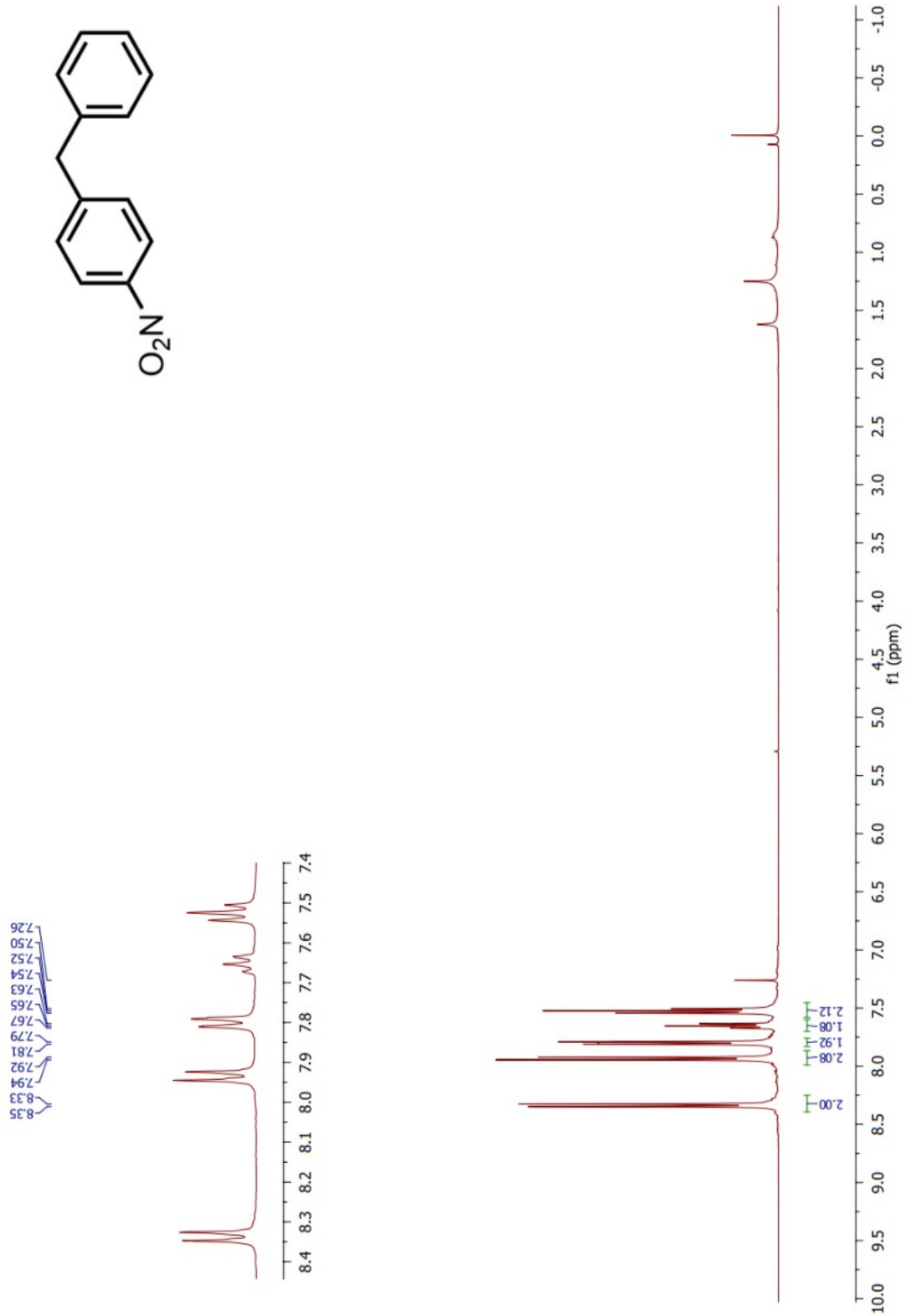

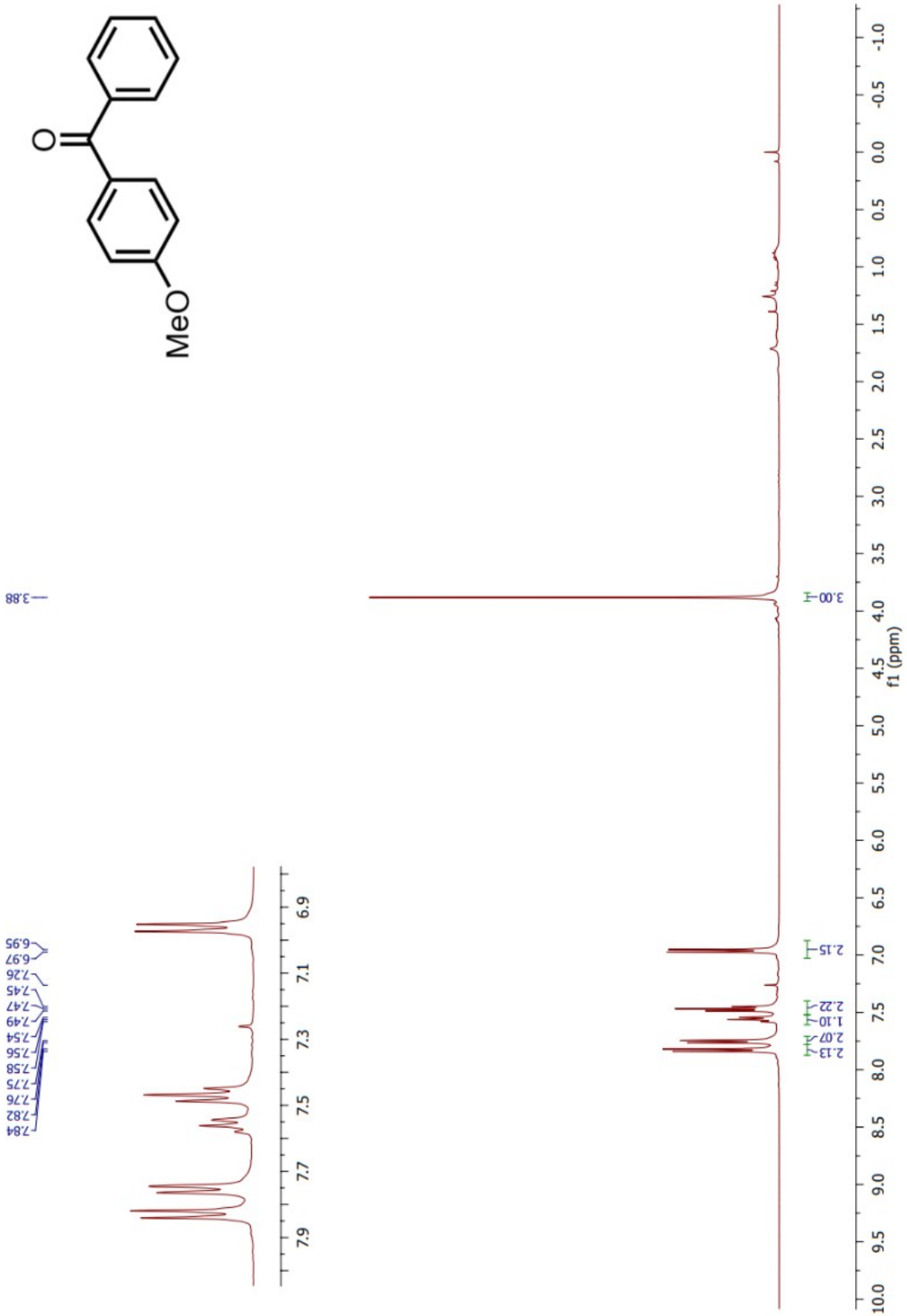

*Proton NMR 8: ^{1}H-NMR spectrum of **21a** in $CDCl_3$.*

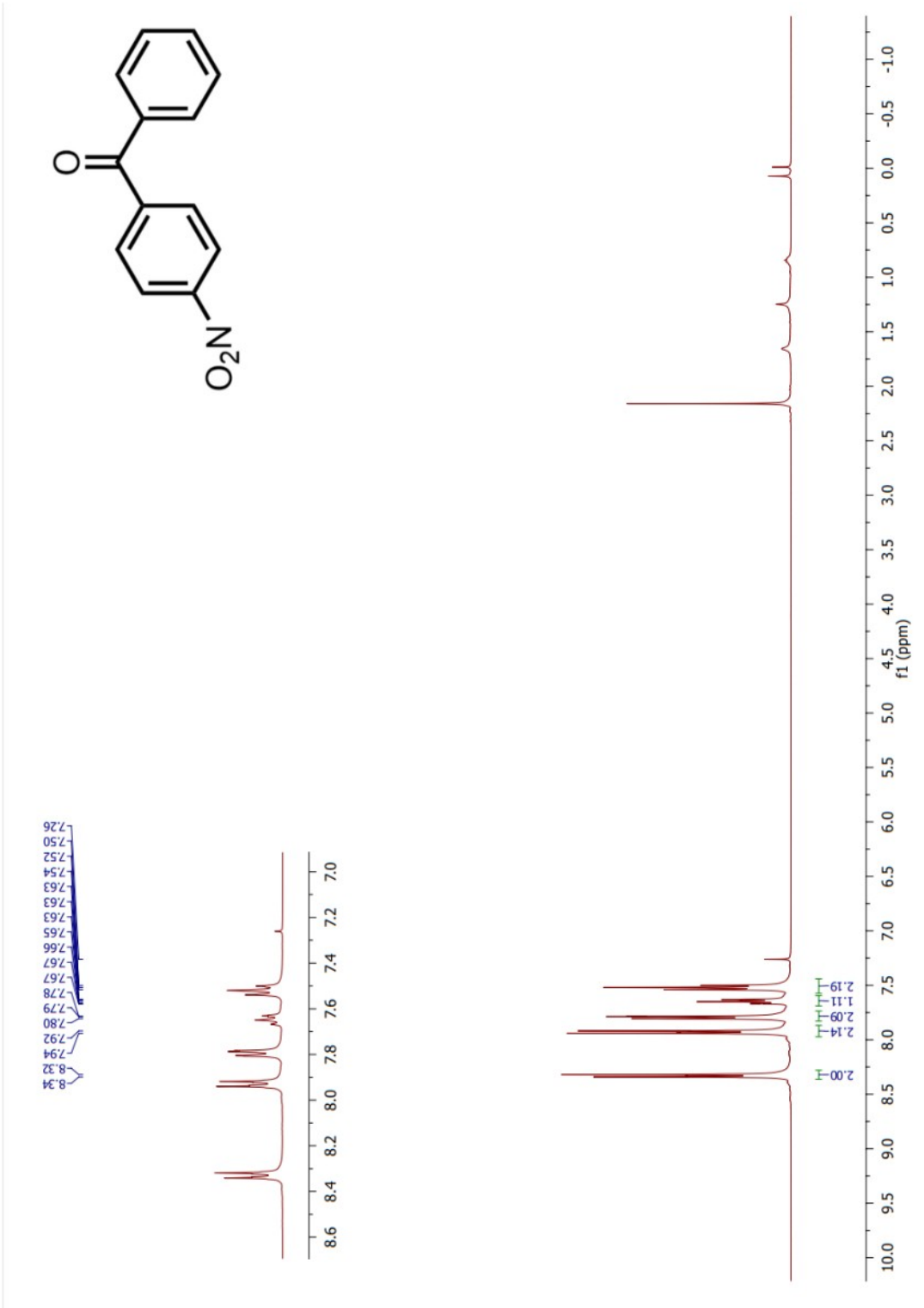

*Proton NMR 9: ^{1}H-NMR spectrum of **21b** in $CDCl_3$.*

REFERENCES:

(1) Tsujimoto, H.; Ha, D.-G.; Markopoulos, G.; Chae, H. S.; Baldo, M. A.; Swager, T. M. Thermally Activated Delayed Fluorescence and Aggregation Induced Emission with Through-Space Charge Transfer. *J. Am. Chem. Soc.* **2017**, *139* (13), 4894–4900. https://doi.org/10.1021/jacs.7b00873.

(2) Miranda-Salinas, H.; Hung, Y.-T.; Chen, Y.-S.; Luo, D.; Kao, H.-C.; Chang, C.-H.; Wong, K.-T.; Monkman, A. Controlling Through-Space and through-Bond Intramolecular Charge Transfer in Bridged D–D'–A TADF Emitters. *J. Mater. Chem. C* **2021**, *9* (28), 8819–8833. https://doi.org/10.1039/D1TC02316K.

(3) Ion Exchange Process: History, Evolution and Applications. *Riv. Nuovo Cimento* **2013**, *36* (9), 397–460. https://doi.org/10.1393/ncr/i2013-10092-1.

(4) Misra, R.; Bhattacharyya, S. P. *Intramolecular Charge Transfer: Theory and Applications*; Wiley-VCH Verlag GmbH & Co. KGaA: Weinheim, Germany, 2018. https://doi.org/10.1002/9783527801916.

(5) Coppola, F.; Cimino, P.; Perrella, F.; Crisci, L.; Petrone, A.; Rega, N. Electronic and Vibrational Manifold of Tetracyanoethylene–Chloronaphthalene Charge Transfer Complex in Solution: Insights from TD-DFT and Ab Initio Molecular Dynamics. *J. Phys. Chem. A* **2022**, *126* (40), 7179–7192. https://doi.org/10.1021/acs.jpca.2c05001.

(6) Kobaisi, M. A.; Bhosale, R. S.; El-Khouly, M. E.; La, D. D.; Padghan, S. D.; Bhosale, S. V.; Jones, L. A.; Antolasic, F.; Fukuzumi, S.; Bhosale, S. V. The Sensitivity of Donor – Acceptor Charge Transfer to Molecular Geometry in DAN – NDI Based Supramolecular Flower-like Self-Assemblies. *Sci. Rep.* **2017**, *7* (1), 16501. https://doi.org/10.1038/s41598-017-15599-9.

(7) Feng, J.; Chen, X.; Han, Q.; Wang, H.; Lu, P.; Wang, Y. Naphthalene-Based Fluorophores: Synthesis Characterization, and Photophysical Properties. *J. Lumin.* **2011**, *131* (12), 2775–2783. https://doi.org/10.1016/j.jlumin.2011.06.027.

(8) Kumar, S.; Franca, L. G.; Stavrou, K.; Crovini, E.; Cordes, D. B.; Slawin, A. M. Z.; Monkman, A. P.; Zysman-Colman, E. Investigation of Intramolecular Through-Space Charge-Transfer States in Donor–Acceptor Charge-Transfer Systems. *J. Phys. Chem. Lett.* **2021**, *12* (11), 2820–2830. https://doi.org/10.1021/acs.jpclett.1c00265.

(9) Khan, S. A. Charge- Transfer Complexes: A Short Review. **2014**, *1* (2).

(10) Algar, W. R.; De Jong, C. A. G.; Maxwell, E. J.; Atkins, C. G. Demonstration of the Spectrophotometric Complementary Color Wheel Using LEDs and Indicator Dyes. *J. Chem. Educ.* **2016**, *93* (1), 162–165. https://doi.org/10.1021/acs.jchemed.5b00665.

(11) Jara, F.; Mascayano, C.; Rezende, M. C.; Tirapegui, C.; Urzua, A. A Spectral and Molecular Dynamics Simulation Study of β-Cyclodextrin Inclusion Complexes with

Solvatochromic Dyes Derived from Barbituric Acid. *J. Incl. Phenom. Macrocycl. Chem.* **2006**, *54* (1–2), 95–99. https://doi.org/10.1007/s10847-005-4806-5.

(12) Buck, J. T.; Wilson, R. W.; Mani, T. Intramolecular Long-Range Charge-Transfer Emission in Donor–Bridge–Acceptor Systems. *J. Phys. Chem. Lett.* **2019**, *10* (11), 3080–3086. https://doi.org/10.1021/acs.jpclett.9b01269.

(13) Ryu, T.; Miyata, K.; Saigo, M.; Shimoda, Y.; Tsuchiya, Y.; Nakanotani, H.; Adachi, C.; Onda, K. Solvent-Dependent Dual Emission Processes in Charge-Transfer Excited States of Phenothiazine-Triphenyltriazine Conformers. *Chem. Phys. Lett.* **2022**, *809*, 140155. https://doi.org/10.1016/j.cplett.2022.140155.

(14) Sasaki, S.; Drummen, G. P. C.; Konishi, G. Recent Advances in Twisted Intramolecular Charge Transfer (TICT) Fluorescence and Related Phenomena in Materials Chemistry. *J. Mater. Chem. C* **2016**, *4* (14), 2731–2743. https://doi.org/10.1039/C5TC03933A.

(15) Marini, A.; Muñoz-Losa, A.; Biancardi, A.; Mennucci, B. What Is Solvatochromism? *J. Phys. Chem. B* **2010**, *114* (51), 17128–17135. https://doi.org/10.1021/jp1097487.

(16) Karmakar, N. K.; Pandey, S.; Pandey, R. K.; Shukla, S. S. Solvatochromism: A Tool for Solvent Discretion for UV-Vis Spectroscopic Studies. *Appl. Spectrosc. Rev.* **2021**, *56* (6), 513–529. https://doi.org/10.1080/05704928.2020.1838918.

(17) Laage, D.; Thompson, W. H.; Blanchard-Desce, M.; Hynes, J. T. Charged Push−Pull Polyenes in Solution: Anomalous Solvatochromism and Nonlinear Optical Properties. *J. Phys. Chem. A* **2003**, *107* (31), 6032–6046. https://doi.org/10.1021/jp0276597.

(18) Marcus, R. A. Electron Transfer Reactions in Chemistry Theory and Experiment. *J. Electroanal. Chem.* **1997**, *438* (1–2), 251–259. https://doi.org/10.1016/S0022-0728(97)00091-0.

(19) Mulder, W. H.; Párkányi, C. Theory of the Salt Effect on Solvatochromic Shifts And Its Potential Application to the Determination of Ground-State and Excited-State Dipole Moments. *J. Phys. Chem. A* **2002**, *106* (49), 11932–11937. https://doi.org/10.1021/jp026505o.

(20) Das, A.; Ghosh, P.; Dutta, A.; Sen, P. Marcus Inversion Is Observed for Excited State Proton Transfer in the Adiabatic Limit Using Naphthol Based Photoacids. *Chem. Phys. Impact* **2021**, *3*, 100044. https://doi.org/10.1016/j.chphi.2021.100044.

(21) Silverstein, T. P. Marcus Theory: Thermodynamics CAN Control the Kinetics of Electron Transfer Reactions. *J. Chem. Educ.* **2012**, *89* (9), 1159–1167. https://doi.org/10.1021/ed1007712.

(22) Ahmadli, D.; Sahin, Y.; Calikyilmaz, E.; Şahin, O.; Türkmen, Y. E. Rapid Access to Hydroxyfluoranthenes via a Domino Suzuki–Miyaura/Intramolecular Diels–Alder/Ring-Opening Reactions Sequence. *J. Org. Chem.* **2022**, *87* (9), 6336–6346. https://doi.org/10.1021/acs.joc.1c03080.

(23) Borisova, K. K.; Kvyatkovskaya, E. A.; Nikitina, E. V.; Aysin, R. R.; Novikov, R. A.; Zubkov, F. I. Classical Example of Total Kinetic and Thermodynamic Control: The Diels–Alder Reaction between DMAD and Bis-Furyl Dienes. *J. Org. Chem.* **2018**, *83* (8), 4840–4850. https://doi.org/10.1021/acs.joc.8b00336.

(24) Thompson, W. H.; Blanchard-Desce, M.; Hynes, J. T. Two Valence Bond State Model for Molecular Nonlinear Optical Properties. Nonequilibrium Solvation Formulation. *J. Phys. Chem. A* **1998**, *102* (39), 7712–7722. https://doi.org/10.1021/jp981916j.

(25) Fromherz, P. Monopole-Dipole Model for Symmetrical Solvatochromism of Hemicyanine Dyes. *J. Phys. Chem.* **1995**, *99* (18), 7188–7192. https://doi.org/10.1021/j100018a061.

(26) Dalton, T.; Faber, T.; Glorius, F. C–H Activation: Toward Sustainability and Applications. *ACS Cent. Sci.* **2021**, *7* (2), 245–261. https://doi.org/10.1021/acscentsci.0c01413.

(27) Altus, K. M.; Love, J. A. The Continuum of Carbon–Hydrogen (C–H) Activation Mechanisms and Terminology. *Commun. Chem.* **2021**, *4* (1), 173. https://doi.org/10.1038/s42004-021-00611-1.

(28) Dhawa, U.; Kaplaneris, N.; Ackermann, L. Green Strategies for Transition Metal-Catalyzed C–H Activation in Molecular Syntheses. *Org. Chem. Front.* **2021**, *8* (17), 4886–4913. https://doi.org/10.1039/D1QO00727K.

(29) Su, B.; Cao, Z.-C.; Shi, Z.-J. Exploration of Earth-Abundant Transition Metals (Fe, Co, and Ni) as Catalysts in Unreactive Chemical Bond Activations. *Acc. Chem. Res.* **2015**, *48* (3), 886–896. https://doi.org/10.1021/ar500345f.

(30) Hunter, B. M.; Gray, H. B.; Müller, A. M. Earth-Abundant Heterogeneous Water Oxidation Catalysts. *Chem. Rev.* **2016**, *116* (22), 14120–14136. https://doi.org/10.1021/acs.chemrev.6b00398.

(31) Nie, R.; Chen, J.; Chen, M.; Qi, Z.; Goh, T.-W.; Ma, T.; Zhou, L.; Pei, Y.; Huang, W. Aerobic Oxidation of the C–H Bond under Ambient Conditions Using Highly Dispersed Co over Highly Porous N-Doped Carbon. *Green Chem.* **2019**, *21* (6), 1461–1466. https://doi.org/10.1039/C8GC03653E.

(32) Tian, X.; Ren, F.; Zhao, B.; Ren, Y.-L.; Zhao, S.; Wang, J. Nitric Acid-Catalyzed Aerobic Oxidation of Benzylic Sp3 C H Bonds of Isochromans, Xanthenes and 9-Fluorenone under Additive-Free Conditions. *Catal. Commun.* **2018**, *106*, 44–49. https://doi.org/10.1016/j.catcom.2017.12.006.

(33) Zhao, M.; Li, J.; Song, Z.; Desmond, R.; Tschaen, D. M.; Grabowski, E. J. J.; Reider, P. J. A Novel Chromium Trioxide Catalyzed Oxidation of Primary Alcohols to the Carboxylic Acids. *Tetrahedron Lett.* **1998**, *39* (30), 5323–5326. https://doi.org/10.1016/S0040-4039(98)00987-3.

(34) Maciuk, S.; Wood, S. H.; Patel, V. K.; Shapland, P. D. P.; Tomkinson, N. C. O. Peracid Oxidation of Unactivated Sp^3 C–H Bonds: An Important Solvent Effect. *Chem. – Eur. J.* **2023**, *29* (31), e202204007. https://doi.org/10.1002/chem.202204007.

(35) Hayashi, E.; Tamura, T.; Aihara, T.; Kamata, K.; Hara, M. Base-Assisted Aerobic C–H Oxidation of Alkylarenes with a Murdochite-Type Oxide Mg_6MnO_8 Nanoparticle Catalyst. *ACS Appl. Mater. Interfaces* **2022**, *14* (5), 6528–6537. https://doi.org/10.1021/acsami.1c20080.

(36) Gavriilidis, A.; Constantinou, A.; Hellgardt, K.; Hii, K. K. (Mimi); Hutchings, G. J.; Brett, G. L.; Kuhn, S.; Marsden, S. P. Aerobic Oxidations in Flow: Opportunities for the Fine Chemicals and Pharmaceuticals Industries. *React. Chem. Eng.* **2016**, *1* (6), 595–612. https://doi.org/10.1039/C6RE00155F.

(37) Karim, A. V.; Hassani, A.; Eghbali, P.; Nidheesh, P. V. Nanostructured Modified Layered Double Hydroxides (LDHs)-Based Catalysts: A Review on Synthesis, Characterization, and Applications in Water Remediation by Advanced Oxidation Processes. *Curr. Opin. Solid State Mater. Sci.* **2022**, *26* (1), 100965. https://doi.org/10.1016/j.cossms.2021.100965.

(38) He, S.; An, Z.; Wei, M.; Evans, D. G.; Duan, X. Layered Double Hydroxide-Based Catalysts: Nanostructure Design and Catalytic Performance. *Chem. Commun.* **2013**, *49* (53), 5912. https://doi.org/10.1039/c3cc42137f.

(39) Sika-Nartey, A. T.; Sahin, Y.; Ercan, K. E.; Kap, Z.; Kocak, Y.; Erdali, A. D.; Erdivan, B.; Türkmen, Y. E.; Ozensoy, E. Two-Dimensional Bimetallic Hydroxide Nanostructures for Catalyzing Low-Temperature Aerobic C–H Bond Activation in Alkylarene and Alcohol Partial Oxidation. *ACS Appl. Nano Mater.* **2022**, *5* (12), 18855–18870. https://doi.org/10.1021/acsanm.2c04634.

(40) Atkins, P. W.; De Paula, J.; Keeler, J. *Atkins' Physical Chemistry*, Eleventh edition.; Oxford University Press: Oxford, United Kingdom ; New York, NY, 2018.

(41) Dale, H. J. A.; Leach, A. G.; Lloyd-Jones, G. C. Heavy-Atom Kinetic Isotope Effects: Primary Interest or Zero Point? *J. Am. Chem. Soc.* **2021**, *143* (50), 21079–21099. https://doi.org/10.1021/jacs.1c07351.

(42) Jankowski, S. Application of NMR Spectroscopy in Isotope Effects Studies. In *Annual Reports on NMR Spectroscopy*; Elsevier, 2009; Vol. 68, pp 149–191. https://doi.org/10.1016/S0066-4103(09)06803-3.

(43) Rana, S.; Biswas, J. P.; Paul, S.; Paik, A.; Maiti, D. Organic Synthesis with the Most Abundant Transition Metal–Iron: From Rust to Multitasking Catalysts. *Chem. Soc. Rev.* **2021**, *50* (1), 243–472. https://doi.org/10.1039/D0CS00688B.

(44) Schmid, H. K.; Mader, W. Oxidation States of Mn and Fe in Various Compound Oxide Systems. *Micron* **2006**, *37* (5), 426–432. https://doi.org/10.1016/j.micron.2005.12.004.

(45) Sahin, Y.; Sika-Nartey, A. T.; Ercan, K. E.; Kocak, Y.; Senol, S.; Ozensoy, E.; Türkmen, Y. E. Precious Metal-Free $LaMnO_3$ Perovskite Catalyst with an Optimized Nanostructure for

Aerobic C–H Bond Activation Reactions: Alkylarene Oxidation and Naphthol Dimerization. *ACS Appl. Mater. Interfaces* **2021**, *13* (4), 5099–5110. https://doi.org/10.1021/acsami.0c20490.

(46) Frimer, A. A.; Farkash-Solomon, T.; Aljadeff, G. Mechanism of the Superoxide Anion Radical (O2-) Mediated Oxidation of Diarylmethanes. *J. Org. Chem.* **1986**, *51* (11), 2093–2098. https://doi.org/10.1021/jo00361a030.

(47) Polliotto, V.; Livraghi, S.; Agnoli, S.; Granozzi, G.; Giamello, E. Reversible Adsorption of Oxygen as Superoxide Ion on Cerium Doped Zirconium Titanate. *Appl. Catal. Gen.* **2019**, *580*, 140–148. https://doi.org/10.1016/j.apcata.2019.05.001.

(48) Xu, C.-F.; Xu, M.; Yang, L.-Q.; Li, C.-Y. Synthesis of Allenes via Gold-Catalyzed Intermolecular Reaction of Propargylic Alcohols and Aromatic Compounds. *J. Org. Chem.* **2012**, *77* (6), 3010–3016. https://doi.org/10.1021/jo300147u.

(49) Liu, C.; Achtenhagen, M.; Szostak, M. Chemoselective Ketone Synthesis by the Addition of Organometallics to *N* -Acylazetidines. *Org. Lett.* **2016**, *18* (10), 2375–2378. https://doi.org/10.1021/acs.orglett.6b00842.

(50) Ohsumi, M.; Ito, A.; Nishiwaki, N. Substrate Switchable Suzuki–Miyaura Coupling for Benzyl Ester *vs.* Benzyl Halide. *RSC Adv.* **2018**, *8* (61), 35056–35061. https://doi.org/10.1039/C8RA07841F.